Validity and limitations of the superexchange model for the magnetic properties of Sr_2IrO_4 and Ba_2IrO_4 mediated by the strong spin-orbit coupling

I. V. Solovyev,[1,2,*] V. V. Mazurenko,[2] and A. A. Katanin[3,2]

[1] *Computational Materials Science Unit, National Institute for Materials Science, 1-1 Namiki, Tsukuba, Ibaraki 305-0044, Japan*

[2] *Department of Theoretical Physics and Applied Mathematics, Ural Federal University, Mira str. 19, 620002 Ekaterinburg, Russia*

[3] *Institute of Metal Physics, S. Kovalevskoy Str. 18, 620990 Ekaterinburg, Russia*

(Dated: August 28, 2015)

Abstract

Layered perovskites Sr_2IrO_4 and Ba_2IrO_4 are regarded as the key materials for understanding the properties of magnetic relativistic insulators, mediated by the strong spin-orbit (SO) coupling. One of the most fundamental issues is to which extent these properties can be described by the superexchange (SE) model, formulated in the limit of the large Coulomb repulsion for some appropriately selected pseudospin states, and whether these materials themselves can be classified as Mott insulators. In the present work we address these issues by deriving the relevant models and extracting parameters of these models from the first-principles electronic structure calculations with the SO coupling. First, we construct the effective Hubbard-type model for the magnetically active t_{2g} bands, by recasting the problem in the language of localized Wannier orbitals. Then, we map the so obtained electron model onto the pseudospin model by applying the theory of SE interactions, which is based on the second-order perturbation theory with respect to the transfer integrals. We discuss the microscopic origin of anisotropic SE interactions, inherent to the compass Heisenberg model, and the appearance of the antisymmetric Dzyaloshinskii-Moriya term, associated with the additional rotation of the IrO_6 octahedra in Sr_2IrO_4. In order to solve the pseudospin Hamiltonian problem and evaluate the Néel temperature (T_N), we employ the non-linear sigma model. We have found that, while for Sr_2IrO_4 our value of T_N agrees with the experimental data, for Ba_2IrO_4 it is overestimated by a factor two. We argue that this discrepancy is related to limitations of the SE model: while for more localized t_{2g} states in Sr_2IrO_4 it works reasonably well, the higher-order terms in the perturbation theory expansion play a more important role in the more "itinerant" Ba_2IrO_4, giving rise to the new type of isotropic and anisotropic exchange interactions, which are not captured by the SE model. This conclusion is supported by unrestricted Hartree-Fock calculations for the same electron model, where in the case of Ba_2IrO_4, already on the mean-field level, we were able to reproduce the experimentally observed magnetic ground state, while for Sr_2IrO_4 the main results are essentially the same as in the SE model.

I. INTRODUCTION

$5d$ transition-metal oxides have attracted a considerable attention as a new paradigm of relativistic magnetic materials, whose properties are largely influenced by the strong spin-orbit (SO) coupling, leading to the experimental realization and a number of theoretical proposals for such fascinating phenomena as SO interaction assisted Mott state in Sr_2IrO_4,[1–3] spin-liquid state in $Pr_2Ir_2O_7$ (Ref. 4) and $Na_4Ir_3O_8$ (Refs. 5 and 6), possible existence of topological semimetallic states in pyrochlore iridates,[7] and unusual magnetic ordering in the honeycomb compounds Na_2IrO_3 and Li_2IrO_3,[8–11] which may be relevant to the Kitaev model of bond-dependent anisotropic magnetic coupling.[12]

In this respect, a lot of attention is being focused on the properties of tetravalent iridium oxides (or iridates), originating from the 5/6-filled Ir t_{2g} band, located near the Fermi level. The strong SO interaction splits the atomic t_{2g} states into the fully occupied four-fold degenerate $j = 3/2$ states and twofold (Kramer's) degenerate $j = 1/2$ states, which accommodate one electron. In this sense, there is a clear analogy with the spin-1/2 systems and the problem of interatomic exchange interactions can be formulated in terms of some appropriately selected pseudospin states. In solids, each group of states form the bands, which can, however, overlap with each other. Moreover, since j is the band quantum number in solids, there is always a finite hybridization between these two groups of relativistic states. The $j = 1/2$ electrons experience the on-site Coulomb repulsion and can polarize the occupied $j = 3/2$ shell via the intraatomic exchange interactions. Moreover, the precise division of the t_{2g} states into the $j = 3/2$ and $j = 1/2$ ones depends on the crystal-field splitting, which is typically smaller than the SO coupling. These are the main ingredients, which predetermine the low-energy electronic properties of iridates.

The layered perovskites, Sr_2IrO_4 and Ba_2IrO_4, are typically regarded as the key materials for revealing the basic microscopic mechanisms, which can operate in iridates. They are also used as the benchmark materials for testing the new theoretical models. In this respect, the first and one of the most successful theoretical models for iridates was based on the theory of superexchange (SE) interactions, which is valid in the limit of large on-site Coulomb repulsion and treats the transfer integrals between the relativistic pseudospin states in the second order of perturbation theory.[6,13] This model indeed reveals a rich and very interesting physics, including the bond dependence of the anisotropic exchange couplings

and emergence of large antisymmetric Dzyaloshinskii-Moriya (DM) interactions when the inversion symmetry is broken by the anti-phase rotations of the IrO_6 octahedra in Sr_2IrO_4.

At the same time, there was always a question about how far one can go in applying the SE model for the real iridates. For the layered iridates, this point was risen in Ref. 14, where, using the dynamical mean-field theory (DMFT), the authors of this work have argued that the behavior of both Sr_2IrO_4 and Ba_2IrO_4 retain many aspects of Slater insulators, whose insulating properties are closely related to the existence of the long-range antiferromagnetic (AFM) order. The problem reemerged again recently after the experimental discovery of the magnetic ground state structure of Ba_2IrO_4,[15] which cannot be described by the SE model, at least on the mean-field level.[16] Thus, the questions is whether this problem should be resolved by considering the quantum fluctuation effects, but within the SE model,[16] or revising the SE model itself by including to it some new higher-order terms in the perturbation theory expansion. The answer to this question is not obvious, because in the SE formulation, the effects of the SO coupling are included to the transfer integral. Therefore, the second-order perturbation theory with respect to the transfer integrals automatically means that it treat the SO coupling also only up to the second order. If the SO interaction is large (as in iridates), it can be rather crude approximation, because it does not take into account several important effects, such as the in-plane anisotropy in the uniaxial systems, which may be relevant to the experimentally observed behavior of Sr_2IrO_4 and Ba_2IrO_4. Another interesting point is the value of Néel temperature (T_N), which is remarkably close in both considered systems (about 240 K), and whether this fact can be rationalized on the basis of SE theory.

The main purpose of this work is to critically reexamine abilities of the SE theory for the layered iridates. This is certainly not the first attempt to derive parameters of interatomic exchange interactions using the theory of SE interactions and the basic ideas of this method in the case of the strong SO coupling are well understood today, at least for the models.[13,16–20] Nevertheless, besides the SO coupling, the behavior of interatomic exchange interactions strongly depends on the number of adjustable parameters, used in the model Hamiltonians, such as the on-site Coulomb and exchange interactions, tetragonal crystal-field splitting, and the matrices of transfer integrals. Therefore, we believe that, in the process of derivation of the pseudospin model, it is very important to reduce the number of possible ambiguities by sticking as much as possible to the first-principles electronic structure calculations.

The rest of the article is organizes as follows. In Sec. II we will briefly discuss the main differences of the crystal and electronic structure of Ba_2IrO_4 and Sr_2IrO_4. Then, in Sec. III we will explain our method of the construction of the effective low-energy electron model on the basis of first-principles electronic structure calculations with the SO coupling. This model will be further used in Sec. IV as the staring point for the derivation of the SE Hamiltonian in the basis of pseudospin states. In Sec. V we will discuss results of our calculations of the SE interactions and their implications to the magnetic properties of Ba_2IrO_4 and Sr_2IrO_4 using the non-linear sigma model. Then, in Sec. VI, we will provide a detailed comparison with the results of unrestricted Hartree-Fock (HF) calculations, which do not rely on the perturbation theory, and argue that while for Sr_2IrO_4 the SE theory works reasonably well, for Ba_2IrO_4 it misses several important interactions, which are nonetheless captured by the HF calculations. Finally, in Sec. VII, we will give a brief summary of our work. Details of derivation of the non-linear sigma model for the compass Heisenberg model will be given in the Appendix.

II. MAIN DETAILS OF CRYSTAL AND ELECTRONIC STRUCTURE

In this work we use the experimental structure parameters, reported in Refs. 21 and 22 (at 13 K) for Ba_2IrO_4 and Sr_2IrO_4, respectively. According to these data, Ba_2IrO_4 crystallizes in the undistorted tetragonal $4m/mmm$ structure with the Ir-O-Ir angles in the xy plane being equal to 180°. Sr_2IrO_4 exhibits the additional rotation of IrO_6 octahedra (the space group $I4_1/acd$), which leads to the deformation of the Ir-O-Ir bonds in the xy plane (see Fig. 1). Depending on the Ir site, this rotation can be either clockwise ($+\phi$) or counterclockwise ($-\phi$). The experimental value of the angle ϕ is 12°.[22]

The corresponding electronic structure in the local-density approximation (LDA) with the SO coupling is displayed in Figs. 2 and 3 for Ba_2IrO_4 and Sr_2IrO_4, respectively. In this work we will focus on the behavior of magnetically active Ir t_{2g} bands, located near the Fermi level and separated relatively well from the rest of the spectrum. There are two main differences between Ba_2IrO_4 and Sr_2IrO_4: (i) The Ir t_{2g} band is narrower in Sr_2IrO_4 (the bandwidth is about about 3 and 3.5 eV in Sr_2IrO_4 and Ba_2IrO_4, respectively). This is generally consistent with the additional distortion in Sr_2IrO_4, which leads to the deformation of the Ir-O-Ir bonds; (ii) The Ba $5d$ band in Ba_2IrO_4, which strongly hybridizes and, therefore, has a large weight

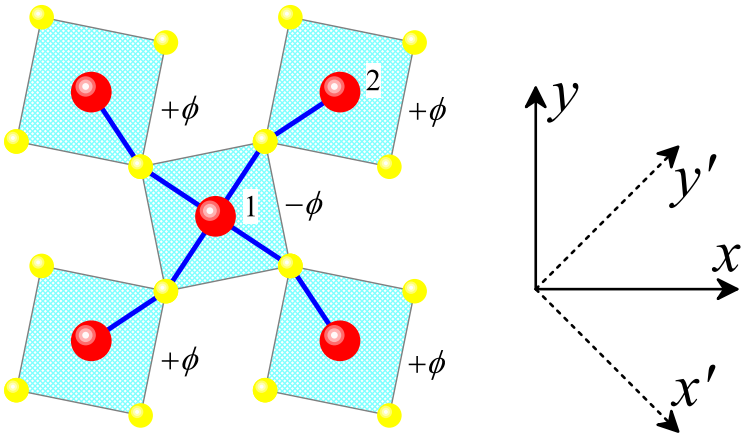

FIG. 1. (Color online) (Left) Rotations of IrO_6 octahedra in the xy plane of Sr_2IrO_4. The Ir atoms are indicated by the big (red) spheres and the oxygen atoms are indicated by the small (yellow) spheres. The sites around which the octahedra are rotated clockwise ($+\phi$) and counterclockwise ($-\phi$) are denoted as 1 and 2, respectively. (Right) The directions of axes in the $I4_1/acd$ (x, y) and $4m/mmm$ (x', y') coordinate frames.

of the Ir $5d$ states, is much closer to the Fermi energy than the Sr $4d$ band in Sr_2IrO_4. This is mainly related to the larger Ba $5d$ bandwidth, due to the less distorted crystal structure as well as the relativistic effects.[23]

In Ba_2IrO_4, the relativistic $j = 3/2$ and $j = 1/2$ subbands are separated by the direct gap, which allows us to construct both 6- and 2-orbitals models (for the entire t_{2g} bands and $j = 1/2$ subband, respectively). In Sr_2IrO_4, due to the additional mixing between the $j = 3/2$ and $j = 1/2$ states, caused by the $I4_1/acd$ distortion, such separation does not take place. Therefore, for Sr_2IrO_4, we will focus only on the 6-orbital model.

III. CONSTRUCTION OF EFFECTIVE LOW-ENERGY ELECTRON MODEL

In this section we will discuss the construction of the low-energy electron model, starting from the LDA band structure with the SO interaction. For practical calculations, we use the linear muffin-tin orbital (LMTO) method in the nearly orthogonal representation.[24] The model itself has the following form:

$$\hat{\mathcal{H}}_{\rm el} = \sum_{ij}\sum_{\alpha\beta} t_{ij}^{\alpha\beta}\hat{c}_{i\alpha}^{\dagger}\hat{c}_{j\beta} + \frac{1}{2}\sum_{i}\sum_{\alpha\beta\gamma\delta} U_{\alpha\beta\gamma\delta}\hat{c}_{i\alpha}^{\dagger}\hat{c}_{i\gamma}^{\dagger}\hat{c}_{i\beta}\hat{c}_{i\delta}, \quad (1)$$

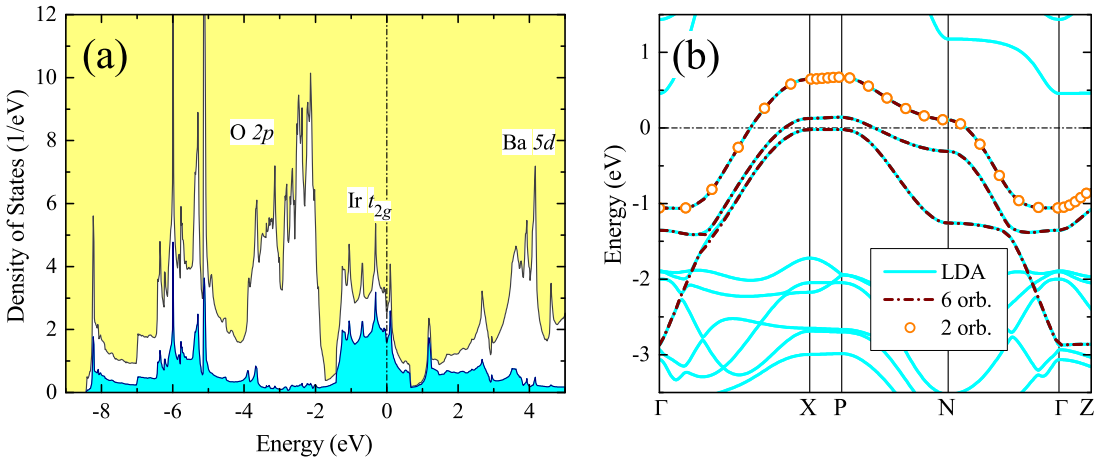

FIG. 2. (Color online) Electronic structure of Ba_2IrO_4 in LDA with the SO coupling. (a) Total and partial densities of states. The shaded area shows the contributions of the Ir $5d$ states. The positions of the main bands are indicated by symbols. (b) Band dispersion near the Fermi level, as obtained for the full LDA Hamiltonian in comparison with the six- and two-orbital models. The high-symmetry points of the Brillouin zone are denoted as $\Gamma = (0,0,0)$, $\mathrm{X} = (\pi/a, \pi/a, 0)$, $\mathrm{N} = (\pi/a, 0, \pi/c)$, $\mathrm{P} = (\pi/a, \pi/a, \pi/c)$, and $\mathrm{Z} = (0,0,2\pi/c)$. The Fermi level is at zero energy (shown by dot-dashed line).

where $\hat{c}^{\dagger}_{i\alpha}$ and $\hat{c}_{i\alpha}$ are, respectively, the creation and annihilation operators of an electron on the Wannier orbitals $w_{i\alpha}$, centered at the Ir site i and specified by the index $\alpha = (m, s)$, which numbers Kramer's doublets m= 1, 2, or 3 (an analog of orbital indices without SO coupling) and the states s= 1 or 2 within each such doublet (an analog of spin indices without SO coupling).

First, we construct the Wannier functions for the magnetically active bands, using the projector-operator technique.[25–27] We consider the 6-orbital model for the both Ba_2IrO_4 and Sr_2IrO_4. Moreover, for Ba_2IrO_4 it is also possible to construct the 2-orbital model, by considering only two highest degenerate bands (see Fig. 2). The trial functions, which are used for the projection, were obtained from the digonalization of the site-diagonal density matrix, calculated for the magnetically active bands in the basis of Ir $5d$ orbitals.[25,27] Namely, after the diagonalization of the density matrix, we pick up either 6 or 2 eigenstates (depending on the dimensionality of the model) with the largest eigenvalues and use them as the trial functions. Such construction guarantees that the Wannier functions are well

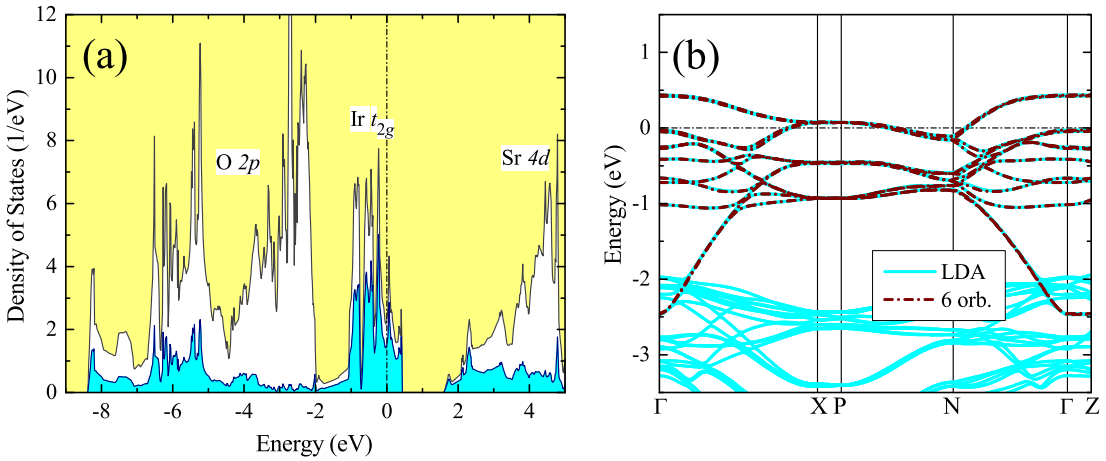

FIG. 3. (Color online) Electronic structure of Sr_2IrO_4 in LDA with the SO coupling. (a) Total and partial densities of states. The shaded area shows the contributions of the Ir $5d$ states. The positions of the main bands are indicated by symbols. (b) Band dispersion near the Fermi level, as obtained for the full LDA Hamiltonian in comparison the six-orbital models. The Fermi level is at zero energy (shown by dot-dashed line).

localized in the real space: the main part of the density matrix with the largest eigenvalues is described by the "heads" of the Wannier functions, residing on the central site, and only small remaining part of this matrix is described by the "tails" of the Wannier functions, coming from the neighboring Ir sites. Thus, the main weight of the Wannier function is concentrated in its "head" part, while the contribution of "tails" is relatively small. Such procedure was extensively used in nonrelativistic calculations without the SO coupling.[25] The new aspect of the relativistic formulation is that the eigenstates of the density matrix become Kramers degenerate. Therefore, the trial functions and the Wannier functions (w_1 and w_2) for each Kramer's doublet can be chosen so to satisfy the conditions: $|w_2\rangle = \hat{T}|w_1\rangle$ and $|w_1\rangle = -\hat{T}|w_2\rangle$, where $\hat{T} = i\hat{\sigma}_y\hat{K}$ is the time-reversal operation, written in terms of the spin Pauli matrix $\hat{\sigma}_y$ and the complex conjugation operator $\hat{K}$.

Then, the one-electron part of the model Hamiltonian (1) is identified with the matrix elements of the LDA Hamiltonian in the Wannier basis: $t_{ij}^{\alpha\beta} = \langle w_{i\alpha}|\hat{\mathcal{H}}_{LDA}|w_{j\beta}\rangle$. This procedure can be also reformulated as the downfolding of the LDA Hamiltonian.[25,27] Then, the site-diagonal matrix elements $t_{i=j}^{\alpha\beta}$ describe the splitting of the atomic levels by the crystal field and the SO interaction, while the off-diagonal elements $t_{i\neq j}^{\alpha\beta}$ stand for interatomic

transfer integrals (or kinetic hoppings).

The matrix of screened on-site interactions $\hat{U} = [U_{\alpha\beta\gamma\delta}]$ has been calculated using simplified version of the constrained random-phase approximation (RPA).[25] The RPA is used in the GW method in order to evaluate the momentum and frequency dependence of the screened Coulomb interaction, which is then used in the calculations of the self-energy.[28] The basic idea of constrained RPA is to switch off some contributions to the RPA polarization function (and, therefore, to the screening of $\hat{U}$) related to the transition between the magnetically active bands (in our case, the Ir $5d$ bands).[29] The RPA is inadequate for this channel of screening (especially when it is evaluated starting from the LDA bandstructure) and should be replaced by a more rigorous method in the process of solution of the low-energy model (1). The purpose of additional simplifications is to replace the time-consuming RPA for the screening, caused by the relaxation of the atomic wavefunction and other (non-$5d$) states, by much faster and more suitable for these purposes constrained LDA technique. After that, we consider (within RPA) the additional and most efficient channel of screening of the Coulomb interactions in the Ir $5d$ bands by (the same) Ir $5d$ states, which contribute to other parts of the electronic structure (mainly to the O $2p$ and either Ba $5d$ or Sr $4d$ bands in Figs. 2 and 3) due to the hybridization.[25] Such approximation incorporates the main channels of screening and, thus, reproduces reasonably well the values of static Coulomb interactions, obtained in full-scale constrained RPA calculations. The obtained matrix elements $U_{\alpha\beta\gamma\delta}$ have the following form:

$$U_{\alpha\beta\gamma\delta} = \int d\mathbf{r} \int d\mathbf{r}' w_\alpha^\dagger(\mathbf{r}) w_\beta(\mathbf{r}) v_{\rm scr}(\mathbf{r},\mathbf{r}') w_\gamma^\dagger(\mathbf{r}') w_\delta(\mathbf{r}'), \tag{2}$$

where the screened interaction $v_{\rm scr}(\mathbf{r},\mathbf{r}')$ in RPA is invariant under the time-reversal operation and does not depend on the spin variables.

IV. PSEUDOSPIN MODEL

In this section we will consider the mapping of the electron model (1) onto the magnetic model, formulated in terms of *pseudospin* variables $\boldsymbol{\mathcal{S}}_i = (\mathcal{S}_i^x, \mathcal{S}_i^y, \mathcal{S}_i^z)$:

$$\hat{\mathcal{H}}_{\mathcal{S}} = \sum_{i>j} \boldsymbol{\mathcal{S}}_i \overleftrightarrow{\boldsymbol{J}}_{ij} \boldsymbol{\mathcal{S}}_j + \sum_i \boldsymbol{\mathcal{S}}_i \overleftrightarrow{\boldsymbol{g}}_i \boldsymbol{H}, \tag{3}$$

where $\overleftrightarrow{\boldsymbol{J}}_{ij}$ and $\overleftrightarrow{\boldsymbol{g}}_i$ are the 3×3 tensors, describing interactions in the system of pseudospins and with the external magnetic field $\boldsymbol{H}$, respectively. The pseudospin operators are represented by the Pauli matrices: $\mathcal{S}_i^x = \frac{1}{2}\begin{pmatrix} 0 & 1 \\ 1 & 0 \end{pmatrix}$, $\mathcal{S}_i^y = \frac{1}{2}\begin{pmatrix} 0 & -i \\ i & 0 \end{pmatrix}$, and $\mathcal{S}_i^z = \frac{1}{2}\begin{pmatrix} 1 & 0 \\ 0 & -1 \end{pmatrix}$.

For each bond, $\overleftrightarrow{\boldsymbol{J}}_{ij}$ can be presented as the sum of its symmetric (S) and antisymmetric (A) components: $\overleftrightarrow{\boldsymbol{J}}_{ij} = \overleftrightarrow{\boldsymbol{J}}_{ij}^{(S)} + \overleftrightarrow{\boldsymbol{J}}_{ij}^{(A)}$, where $\overleftrightarrow{\boldsymbol{J}}_{ij}^{(S)} = \frac{1}{2}(\overleftrightarrow{\boldsymbol{J}}_{ij} + \overleftrightarrow{\boldsymbol{J}}_{ij}^T)$ and $\overleftrightarrow{\boldsymbol{J}}_{ij}^{(A)} = \frac{1}{2}(\overleftrightarrow{\boldsymbol{J}}_{ij} - \overleftrightarrow{\boldsymbol{J}}_{ij}^T)$. The part $\overleftrightarrow{\boldsymbol{J}}_{ij}^{(S)}$ incorporates all types of symmetric exchange interactions and its trace is the isotropic exchange interaction in the bond i-j: $J_{ij} = \mathrm{Tr}\overleftrightarrow{\boldsymbol{J}}_{ij}^{(S)}$, while $\overleftrightarrow{\boldsymbol{J}}_{ij}^{(A)}$ describes anisotropic DM interactions. $\overleftrightarrow{\boldsymbol{J}}_{ij}^{(A)}$ has only three independent elements, which can be viewed as the components of some axial vectors (the so-called DM vector) $\boldsymbol{d}_{ij} = (d_{ij}^x, d_{ij}^y, d_{ij}^z)$:

$$\overleftrightarrow{\boldsymbol{J}}_{ij}^{(A)} = \begin{pmatrix} 0 & d_{ij}^z & -d_{ij}^y \\ -d_{ij}^z & 0 & d_{ij}^x \\ d_{ij}^y & -d_{ij}^x & 0 \end{pmatrix},$$

yielding the well known identity: $\boldsymbol{\mathcal{S}}_i\overleftrightarrow{\boldsymbol{J}}_{ij}^{(A)}\boldsymbol{\mathcal{S}}_j = \boldsymbol{d}_{ij}[\boldsymbol{\mathcal{S}}_i \times \boldsymbol{\mathcal{S}}_j]$.

A. Calculation of superexchange interactions

In order to calculate the SE interactions, we adapt a standard procedure for the systems, whose degeneracy in the atomic limit is lifted by the crystal field and SO interaction. Namely, we assume that, in the atomic limit, the single hole resides on the highest Kramer's doublet, obtained from the diagonalization of the site-diagonal part $\hat{t} = [t_{i=j}^{\alpha\beta}]$ of the one-electron Hamiltonian. The states $|\varphi_1\rangle$ and $|\varphi_2\rangle$ of this Kramer's doublet are used for the construction of eigenstates $|\pm x\rangle$, $|\pm y\rangle$, and $|\pm z\rangle$ of the pseudospin operators $\mathcal{S}^x$, $\mathcal{S}^y$, and $\mathcal{S}^z$, respectively. For convenience, we choose the phases of these states so that $|\varphi_2\rangle = \hat{T}|\varphi_1\rangle$ and $|\varphi_1\rangle = -\hat{T}|\varphi_2\rangle$.

Let us first explain the construction for $|\pm z\rangle$. For these purposes, one can choose any pair of states, which is obtained by the unitary transformation of $|\varphi_1\rangle$ and $|\varphi_2\rangle$. Moreover, since the states are degenerate, the transformation will not change the total energy, and the model (3) will not contain the single-ion anisotropy term. Then, we employ the fact that, despite some complications caused by the strong SO coupling, the magnetic moment will always have a finite spin component, and define the pseudospin states $|+z\rangle$ and $|-z\rangle$ as

those corresponding to, respectively, the maximal and minimal projections of spin onto the z axis. The problem is equivalent to the diagonalization of the 2×2 spin Pauli matrix $\hat{\sigma}_z$ in the basis of $|\varphi_1\rangle$ and $|\varphi_2\rangle$.

Then, one can readily define two other groups of states as $|\pm x\rangle = \frac{1}{\sqrt{2}}|+z\rangle \pm \frac{1}{\sqrt{2}}|-z\rangle$ and $|\pm y\rangle = \pm\frac{1-i}{2}|+z\rangle + \frac{1+i}{2}|-z\rangle$. In this construction, the phases of $|\pm z\rangle$ were chosen to satisfy the condition: $\hat{T}|-z\rangle = |+z\rangle$ and $\hat{T}|+z\rangle = -|-z\rangle$. It allows us to define unambiguously all phases of $|\pm z\rangle$ but ζ, which transforms $|\pm z\rangle$ to $e^{\mp i\zeta}|\pm z\rangle$. The latter phase is defined so to satisfy the condition $\langle +x|\hat{\sigma}_y|+x\rangle = 0$.

In order to find $\overleftrightarrow{\boldsymbol{J}}_{ij}$, we evaluate the energy gain $\mathcal{T}_{ij}(a,b)$, caused by the virtual excitations of the hole from the a-th orbital of the site i to the b-th orbital of the site j and vice versa, in the second order of perturbation theory with respect to the transfer integrals $t^{\alpha\beta}_{i\neq j}$. The denominators in the SE theory are given by the energies of charge excitations $d_i^5 d_j^5 \rightarrow d_i^4 d_j^6$, which are the energies of the two-hole states. In the process of virtual excitations, the Pauli exclusion principle was guaranteed by the projection operators, which permit the hoppings only between occupied and unoccupied orbitals. Moreover, for the excited two-hole states, the problem was solved in the true many-body fashion, by finding the eigenstates and the eigenenergies from the diagonalization of the Coulomb interaction matrix $\hat{U}$ in the basis of $\frac{6\times 5}{2} = 15$ Slater determinants, constructed from 6 atomic orbitals. This is a step beyond the mean-field approximation, which additionally stabilizes the AFM interactions.[25] Then, we consider all combinations of a and $b = \pm x$, $\pm y$, or $\pm z$, and map the obtained energy gains onto the pseudospin model (3) for $\boldsymbol{H} = 0$. This procedure was discussed in details in Ref. 30.

B. Calculation of g-tensor

The g-tensor describes the interaction of the pseudopsin with the external magnetic field [see Eq. (3)]. It can be evaluated using Eq. (31.34) of Ref. 31, from which one can find all 9 elements of the tensor $\overleftrightarrow{\boldsymbol{g}}$ at each site of the lattice: $\langle +z|(L_x + \sigma_x)|+z\rangle = g^{xz}$, $\langle +z|(L_y + \sigma_y)|+z\rangle = g^{yz}$, $\langle +z|(L_z+\sigma_z)|+z\rangle = g^{zz}$, $\langle -z|(L_x+\sigma_x)|+z\rangle = g^{xx}+ig^{xy}$, $\langle -z|(L_y+\sigma_y)|+z\rangle = g^{yx} + ig^{yy}$, and $\langle -z|(L_z + \sigma_z)|+z\rangle = g^{zx} + ig^{zy}$, where L_x, L_y, and L_z are the matrices of angular momentum operators in the Wannier basis. It is easy to separate the spin $\overleftrightarrow{\boldsymbol{g}}_S$ and orbital $\overleftrightarrow{\boldsymbol{g}}_L$ contributions to the g-tensor, by considering the matrix elements of only $\boldsymbol{\sigma}$ and

$\boldsymbol{L}$, respectively.

V. RESULTS AND DISCUSSIONS

A. Two-orbital model for Ba_2IrO_4

The two-orbital model is the simplest model, which can be considered. In Ba_2IrO_4, the "$j = 1/2$" bands are separated from the rest of the spectrum (see Fig. 2) and the construction is rather straightforward.

The form of transfer integrals in this case is very simple. Since $\hat{t}$ is hermitian, each 2×2 matrix $\hat{t}_{ij} = [\hat{t}_{ij}^{\alpha\beta}]$ satisfies the property: $\hat{t}_{ji} = \hat{t}_{ij}^{\dagger}$. Then, since all Ir sites are located in the inversion centers and connected by the translations, it holds $\hat{t}_{ji} = \hat{t}_{ij}$ and, therefore, $\hat{t}_{ij} = \hat{t}_{ij}^{\dagger}$. Finally, since $\hat{\mathcal{H}}_{LDA}$ is invariant under the time-reversal operation, we will have two more identities: $(t_{ij}^{11})^* = t_{ij}^{22}$ and $(t_{ij}^{12})^* = -t_{ij}^{21}$, which can be obtained from $(t_{ij}^{\alpha\beta})^* = \langle \hat{T} w_{i\alpha} | \hat{T} \hat{\mathcal{H}}_{LDA} | w_{j\beta} \rangle$. Thus, in the two-orbital model, each $\hat{t}_{ij}$ is proportional to the unity matrix $\hat{t}_{ij} = t_{ij}\hat{1}$ in the subspace spanned by the indices $\alpha(\beta) = 1$ and 2, where t_{ij} is a real constant.

The behavior of t_{ij} is explained in Fig. 4. As expected, the strongest hopping occurs between nearest neighbors in the xy plane. There are also finite hoppings between next-nearest neighbors in and between the planes.

Since $\hat{t}_{ij} = t_{ij}\hat{1}$, all SE interactions in the two-orbital model are isotropic. They can be easily evaluated using the formula $J_{ij} = 4t_{ij}^2/\mathcal{U}$,[32] where $\mathcal{U} = 1.52$ eV is the effective on-site Coulomb repulsion, obtained in the constrained RPA for the two-orbital model. Then, using the values of transfer integrals, which are displayed in Fig. 4, we will obtain $J_{ij} =$ 122.8, 2.5, and 0.8 meV for the nearest-neighbor (NN), next-NN, and interplane interactions, respectively. Since $J_{ij} > 0$, all interactions are antiferromagnetic.

B. Six-orbital model for Ba_2IrO_4

The atomic t_{2g} states are split into three doubly degenerate groups of levels, which in Ba_2IrO_4 are located at −209, −149, and 358 meV, relative to their center of gravity. Two lowest doublets correspond to $j = 3/2$, and the highest one – to $j = 1/2$. Thus, the splitting between the $j = 1/2$ and $j = 3/2$ states, which measures the strength of the SO

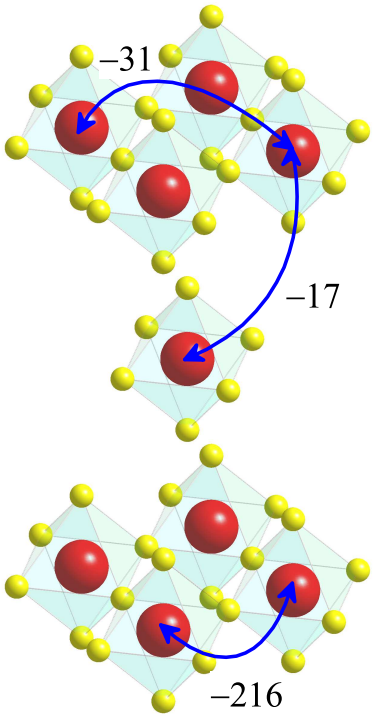

FIG. 4. (Color online) Crystal structure and transfer integrals (in meV) associated with different Ir-Ir bonds in the two-orbital model for Ba_2IrO_4. The Ir atoms are indicated by the big (red) spheres and the oxygen atoms are indicated by the small (yellow) spheres.

coupling is very large. This justifies the use of the regular (nondegenerate) theory for the SE interactions.

For the tetragonal compounds, the eigenstates $|+z\rangle$ (and $|-z\rangle = -\hat{T}|+z\rangle$), corresponding to the highest Kramer's doublet, can be decomposed in the basis of xy, yz, zx, and x^2-y^2 Wannier orbitals with both projection of spins:

$$|+z\rangle = c^{\uparrow}_{xy}|w_{xy,\uparrow}\rangle + c^{\uparrow}_{yz}|w_{yz,\uparrow}\rangle + c^{\uparrow}_{zx}|w_{zx,\uparrow}\rangle + c^{\uparrow}_{x^2-y^2}|w_{x^2-y^2,\uparrow}\rangle + c^{\downarrow}_{xy}|w_{xy,\downarrow}\rangle + c^{\downarrow}_{yz}|w_{yz,\downarrow}\rangle + c^{\downarrow}_{zx}|w_{zx,\downarrow}\rangle + c^{\downarrow}_{x^2-y^2}|w_{x^2-y^2,\downarrow}\rangle. \quad (4)$$

Due to the symmetry constraint, the $3z^2-r^2$ orbitals do not contribute to $|+z\rangle$. The coefficients in this expansion depend on the relative strength of the crystal-field splitting and the SO interaction. They cannot be determined solely from the symmetry principles. For Ba_2IrO_4, we obtain the following (nonvanishing) coefficients in the original $I4/mmm$ coordinate frame: $c^{\downarrow}_{x'y'} = -i0.522$, $c^{\uparrow}_{z'x'} = -ic^{\uparrow}_{y'z'} = 0.603$, and $c^{\downarrow}_{x'^2-y'^2} = -0.004$, which correspond to $c^{\downarrow}_{xy} = 0.004$, $c^{\uparrow}_{zx} = -ic^{\uparrow}_{yz} = 0.426 + i0.426$, and $c^{\downarrow}_{x^2-y^2} = -i0.522$ in the $I4_1/acd$ frame.

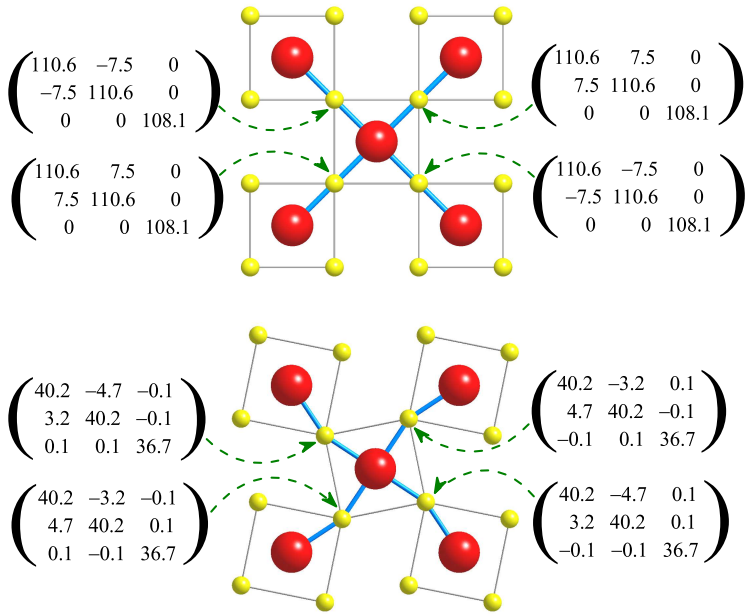

FIG. 5. (Color online) Tensors of superexchange interactions $\overleftrightarrow{\boldsymbol{J}}_{ij}$ (in meV), associated with different Ir-Ir bonds in the xy plane of Ba_2IrO_4 (top) and Sr_2IrO_4 (bottom). The Ir atoms are indicated by the big (red) spheres and the oxygen atoms are indicated by the small (yellow) spheres. For the sake of convenience, the parameters for both structures are shown in the $I4_1/acd$ coordinate frame.

The strongest transfer integrals, operating between the nearest neighbors in the xy plane, have the following form (in meV):

$$\hat{t}_{\langle ij\rangle||x',y'} = \begin{pmatrix} -283 & 0 & 0 & \pm 60 & 0 & -i76 \\ 0 & -283 & \mp 60 & 0 & -i76 & 0 \\ 0 & \mp 60 & -165 & 0 & \pm i92 & 0 \\ \pm 60 & 0 & 0 & -165 & 0 & \mp i92 \\ 0 & i76 & \mp i92 & 0 & -226 & 0 \\ i76 & 0 & 0 & \pm i92 & 0 & -226 \end{pmatrix}, \tag{5}$$

where the upper (lower) sign stands for the bonds parallel to the x' (y') axis in the $I4/mmm$ coordinate frame (see Fig. 5). Here, the matrix is given in the local representation, which diagonalizes the site-diagonal part of the one-electron Hamiltonian $[\hat{t}_{i=j}]$, as described in Sec. IV A. Moreover, we adapt the following order of the Wannier orbitals: (m, s)= $(1, 1)$, $(1, 2)$, $(2, 1)$, $(2, 2)$, $(3, 1)$, and $(3, 2)$, where m numbers the Kramer's doublet in the increasing

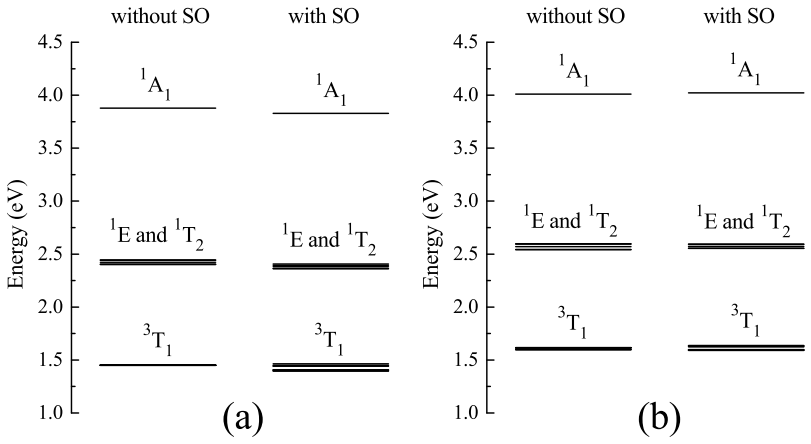

FIG. 6. The energies of two-hole states for Ba_2IrO_4 (a) and Sr_2IrO_4 (b), obtained using parameters of screened Coulomb interactions $U_{\alpha\beta\gamma\delta}$ for the six-orbital model with and without the spin-orbit (SO) coupling.

order of their energies and s number the states within each doublet. Similar to the 2-orbital model, the matrix elements of $\hat{t}_{ij}$ with same m do not depend on the s-indices and each such sub-block is proportional to the 2×2 unity matrix. However, there is a finite coupling between states with different m's. This coupling gives rises to the anisotropy of $\overleftrightarrow{\boldsymbol{J}}_{ij}$. Moreover, since the signs of some of these matrix elements alternate between the bonds parallel to the x' and y' axes, the anisotropic part of $\overleftrightarrow{\boldsymbol{J}}_{ij}$ will also alternate in the $x'y'$ plane. Another important factor, which is responsible for anisotropic properties of $\overleftrightarrow{\boldsymbol{J}}_{ij}$ is the intraatomic exchange interaction $\mathcal{J}$.[13] It will be discussed below. Other parameters of the model Hamiltonian can be found elsewhere.[33]

The form of the screened on-site interactions $U_{\alpha\beta\gamma\delta}$ in the basis of relativistic Wannier orbitals is rather complex. Nevertheless, the main details of these interactions can be understood by considering the energies of two-hole excitations, which contribute to the SE processes (see Fig. 6). These energies were calculated using the matrices of screened Coulomb interactions $[U_{\alpha\beta\gamma\delta}]$, for which $v_{\rm scr}(\mathbf{r},\mathbf{r}')$ was obtained for two types of the electronic structures: with and without the SO coupling [see Eq. (2)]. In the case of perfect cubic environment and without the SO coupling, the two-hole states are split into three groups: $^3T_1$, degenerate $^1T_2$ and ^1E, and $^1A_1$ with the energies $(\mathcal{U}-3\mathcal{J})$, $(\mathcal{U}-\mathcal{J})$, and $(\mathcal{U}+2\mathcal{J})$, respectively,[34] in terms of the intraorbital Coulomb interaction $\mathcal{U}$ and the ex-

change interaction $\mathcal{J}$.[35] The tetragonal environment of the Ir^{4+} ions, realized in Ba_2IrO_4, slightly lifts the degeneracy of the $^1T_2$ and ^1E states. The SO interaction further lifts the degeneracy of the $^3T_1$ states. However, in all other respects the positions of the main energy levels in very similar with and without the SO interactions. The (averaged) parameters $\mathcal{U}$ and $\mathcal{J}$ can be evaluated from the centers of gravity of the three groups of levels. This yields: $\mathcal{U} = 2.86$ (2.91) eV and $\mathcal{J} = 0.48$ (0.49) eV with (without) SO interaction. Thus, $\mathcal{U}$ is generally larger in the 6-orbital model, in comparison with the 2-orbital one, due to the additionally screened by the $j = 3/2$ electrons, which is included in the 2-orbital model, but not in the 6-orbital one.

The parameters of NN SE interactions in the xy plane are explained in Fig. 5. Since $J_{ij}^{xx} = J_{ij}^{yy} > J_{ij}^{zz}$, these parameters favor the inplane configuration of the pseudospins, in agreement with the experiment.[15] Moreover, the phase of the off-diagonal element J_{ij}^{xy} (in the $I4_1/acd$ coordinate frame) is bond-dependent, giving rise to the quantum compass interaction term. In the more conventional $I4/mmm$ coordinate frame, the tensor $\overleftrightarrow{\boldsymbol{J}}_{ij}$ is diagonal with the parameters given by $J_{ij}^{x'x'} = J_{ij}^{xx} \pm |J_{ij}^{xy}|$ and $J_{ij}^{y'y'} = J_{ij}^{xx} \mp |J_{ij}^{xy}|$, where the upper (lower) sign stands for the bonds parallel to the x' (y') axis. The isotropic part $J_{ij} = \frac{1}{3}(J_{ij}^{xx}+J_{ij}^{yy}+J_{ij}^{zz}) = 109.8$ meV is close to the value $J_{ij} = 123$ meV, obtained in the 2-orbital model. This is mainly because of the combination of two effects: On the one hand, $\mathcal{U}$ is larger in the 6-orbital model, which should lead to the smaller J_{ij}. This decrease of J_{ij} is partly compensated by somewhat stronger transfer integrals, operating between orbitals belonging to the highest Kramer's doublet (-226 meV instead of -216 meV in the two-orbital model).

As was already mensioned before, there are two important factors, which leads to the anisotropy of $\overleftrightarrow{\boldsymbol{J}}_{ij}$: (i) finite transfer integrals, connecting the states with $j = 3/2$ and $j = 1/2$ [see Eq. 5] and (ii) finite intraatomic exchange coupling $\mathcal{J}$,[13] which lifts the main degeneracy of the virtual two-hole states (see Fig. 6). For instance, using the same transfer integrals, but simplified matrix of the screened on-site Coulomb interactions, which was reconstructed from the parameters of averaged $\mathcal{U} = 2.86$ eV and $\mathcal{J} = 0$, we have obtained totally isotropic tensor $\overleftrightarrow{\boldsymbol{J}}_{ij} \equiv J_{ij}\overleftrightarrow{\mathbf{1}}$, where $\overleftrightarrow{\mathbf{1}}$ is the 3×3 unity tensor and $J_{ij} = 71$ meV.

The direction of the uniaxial anisotropy is also controlled by the tetragonal crystal-field splitting $\Delta_{t_{2g}}$ between $x'y'$ and doubly degenerate $y'z'$ and $z'x'$ orbitals without the SO coupling. If the $x'y'$ orbital was located higher in energy, we would deal with the out-of-

plane configuration of pseudospins: $J_{ij}^{xx} = J_{ij}^{yy} < J_{ij}^{zz}$. Such situation is indeed realized for $\Delta_{t_{2g}} = 107$ meV, associated entirely with the change of the hybridization due to the compression of the IrO_6 octahedra in the $x'y'$ plane. However, the additional nonspherical Madelung interaction (see Ref. 25) yields $\Delta_{t_{2g}} = -69$ meV, thus changing the order of the t_{2g} orbitals and enforcing the in-plane configuration of the pseudospins ($J_{ij}^{xx} = J_{ij}^{yy} > J_{ij}^{zz}$), in agreement with the experimental data.[15] In mathematical terms, it leads to the inequality $|c_{x'y'}^{\downarrow}| < |c_{y'z'}^{\uparrow}|=|c_{z'x'}^{\uparrow}|$ for the coefficients in Eq. (4). It is interesting that for the single-ion anisotropy (if the latter was appropriate in the analysis of some more general magnetic model), the preferential population of the $y'z'$ and $z'x'$ orbitals typically stabilizes the out-of-plane configuration of spin and orbital magnetic moments. However, it should not be confused with the present situation, where we deal with the *intersite* interactions, which are governed by completely different processes rather than the single-ion anisotropy energy. This example emphasizes the importance of the tetragonal crystal-field splitting, which is sometimes ignored during the construction of the pseudospin models.[19]

Due to the tetragonal $I4/mmm$ symmetry, the g-tensor of Ba_2IrO_4 has only two inequivalent matrix elements: $g^{xx} = g^{yy}$ and g^{zz}. Other elements are identically equal to zero. The value of g^{xx} and g^{zz} are listed in Table I together with the partial contributions of the spin and orbital components.

TABLE I. Matrix elements of the g-tensor, obtained in the six-orbital model for Ba_2IrO_4 and Sr_2IrO_4, and results of their decomposition into the spin (S) and orbital (L) parts (given in parenthesis).

Compound	g^{xx} (g_S^{xx}, g_L^{xx})	g^{zz} (g_S^{zz}, g_L^{zz})	g^{xy} (g_S^{xy}, g_L^{xy})
Ba_2IrO_4	1.796 $(0.545, 1.251)$	2.380 $(0.909, 1.470)$	0 $(0, 0)$
Sr_2IrO_4	1.115 $(0.208, 0.907)$	3.332 $(1.582, 1.750)$	0.005 $(0, 0.005)$

C. Six-orbital model for Sr_2IrO_4

In the case of Sr_2IrO_4, the splitting of the t_{2g} levels is -431, -4, and 435 meV. The symmetry properties of the $|+z\rangle$ orbital are given by the same Eq. (4) with the following (nonvanishing) coefficients: $c_{xy}^{\downarrow} = -0.015 \mp i0.087$, $c_{zx}^{\uparrow} = -ic_{yz}^{\uparrow} = \pm 0.184 + i0.643$,

and $c^{\downarrow}_{x^2-y^2} = \pm 0.004 - i0.311$, where the upper (lower) sign is referred to the site 1 (2), experiencing the counterclockwise (clockwise) rotation of the IrO_6 octahedra (see Fig. 1).

In the local representation, which diagonalizes the site-diagonal part $[t^{\alpha\beta}_{i=j}]$ of the one-electron Hamiltonian, the matrix of transfer integrals between sites 1 and 2 in the xy planes is given by (in meV)

$$\hat{t}_{\langle ij\rangle||x',y'} = \begin{pmatrix} 218+i60 & 0 & 0 & \mp 24 \mp i11 & 0 & 4-i38 \\ 0 & 218-i60 & \pm 24 \mp i11 & 0 & -4-i38 & 0 \\ 0 & \mp 24 \pm i11 & -94-i69 & 0 & \pm 29 \mp i68 & 0 \\ \pm 24 \pm i11 & 0 & 0 & -94+i69 & 0 & \pm 29 \pm i68 \\ 0 & -4-i38 & \mp 29 \pm i68 & 0 & -144-i7 & 0 \\ 4-i38 & 0 & 0 & \mp 29 \mp i68 & 0 & -144+i7 \end{pmatrix},$$

where the upper (lower) sign stands for the bond parallel to the x' (y') axis (see Fig. 1 for the notations). This matrix has both hermitian $\hat{t}^{\rm h}_{ij} = \frac{1}{2}(\hat{t}_{ij} + \hat{t}_{ji})$ and antihermitian $\hat{t}^{\rm ah}_{ij} = \frac{1}{2}(\hat{t}_{ij} - \hat{t}_{ji})$ parts. The hermitian part has the same form as in Ba_2IrO_4, where the off-diagonal matrix elements give rise to symmetric anisotropic interactions $\overleftrightarrow{\boldsymbol{J}}^{(S)}_{ij}$. The alternation of signs of some of these matrix elements will also lead to the alternation of anisotropic interactions in the xy plane. The antihermitian part is the new aspect, which is related to the fact that the neighboring Ir sites in the $I4_1/acd$ structure are no longer connected by the inversion operation. This part is responsible for the DM interactions. The transfer integrals, involving the highest Kramer's doublet are generally smaller in Sr_2IrO_4 in comparison with Ba_2IrO_4, mainly due to the additional rotation of the IrO_6 octahedra and deformation of the Ir-O-Ir bonds. Therefore, the SE interactions are also expected to be smaller in Sr_2IrO_4.

Due to the additional symmetry lowering, the matrix of the screened Coulomb interactions $[U_{\alpha\beta\gamma\delta}]$ is even more complex than in Ba_2IrO_4. Nevertheless, the energies of the two-hole states, obtained from $[U_{\alpha\beta\gamma\delta}]$, have the same "three-level" structure as in Ba_2IrO_4, which is only slightly deformed by the lattice distortion and the SO interaction (see Fig. 6). The averaged parameters $\mathcal{U}$ and $\mathcal{J}$ can be again evaluated from the splitting between these three groups of levels as $\mathcal{U} = 3.05$ eV and $\mathcal{J} = 0.48$ eV (both with and without the SO interaction). The value of $\mathcal{J}$ is comparable with the one in Ba_2IrO_4. However, the Coulomb repulsion $\mathcal{U}$ is slightly larger in Sr_2IrO_4. This behavior is consistent with the change of the electronic structure (see Figs. 2 and 3): since the unoccupied Ba $5d$ states are closer to the

Fermi level and strongly hybridize with the Ir $5d$ states, the Coulomb $\mathcal{U}$ is expected to be more screened in Ba_2IrO_4 than in Sr_2IrO_4.[25] Moreover, it is reasonable to expect that the additional $I4_1/acd$ distortion in the case of Sr_2IrO_4 will make the t_{2g} states more localized and, thus, the screening of $\mathcal{U}$ less efficient. This will further reduce the values of the SE interactions in Sr_2IrO_4.

Considering only the values of interorbital Coulomb interactions $\mathcal{U}' = \mathcal{U} - 2\mathcal{J} = 1.90$ eV and 2.09 eV for Ba_2IrO_4 and Sr_2IrO_4, respectively, we note a reasonable agreement with the results full-scale constrained RPA calculations reported in Ref. 14 ($\mathcal{U}'$ is about 1.47 eV and 1.77 eV for Ba_2IrO_4 and Sr_2IrO_4, respectively). Moreover, the authors of Ref. 14 used a simplified $I4/mmm$ structure and theoretical lattice parameters both for Ba_2IrO_4 and Sr_2IrO_4, which may lead to the additional screening of $\mathcal{U}'$. A more serious discrepancy is found for $\mathcal{J}$: our value of $\mathcal{J}$ is close to the atomic one, which seems to be reasonable, because $\mathcal{J}$ is only weakly screened in RPA.[36] However, the values of $\mathcal{J}$ reported in Ref. 14 are about three times smaller, leading to the violation of the Kanamori rule $\mathcal{U}' = \mathcal{U} - 2\mathcal{J}$, presumably due to the contribution of the oxygen states to the Wannier functions.[37] This itself is an interesting point, because, according to Ref. 13, smaller value of $\mathcal{J}$ within the spherical model, which respects the Kanamori rule, should reduce the anisotropy of the exchange interactions. Therefore, it is interesting to which extent this anisotropy of the exchange interactions will be compensated by the anisotropy of the Coulomb interactions, which emerges in the full-scale constrained RPA calculations and manifested in the violation of the Kanamori rule. In any case, according to the analysis of the effective electron model based on the dynamical mean-field theory,[14] our values of the parameters $\mathcal{U}$ and $\mathcal{U}'$ should correspond to the insulating behavior for Ba_2IrO_4 and Sr_2IrO_4, thus justifying the use of the $1/\mathcal{U}$ expansion for the analysis of the exchange interactions.

The $I4_1/acd$ structure of Sr_2IrO_4 contains two IrO_2 planes. The behavior of NN SE interactions in one of the plane is explained in Fig. 5. The parameters in another plane can be obtained by the 90°-rotation about the z-axis. As was expected, the isotropic part of the exchange interactions $J_{12} = \frac{1}{3}(J_{12}^{xx}+J_{12}^{yy}+J_{12}^{zz}) = 39.0$ meV is considerably smaller than in Ba_2IrO_4.

Since $J_{12}^{xx} = J_{12}^{yy} > J_{12}^{zz}$, the pseudospins will favor the in-plane configuration, similar to Ba_2IrO_4 and in agreement with the experimental situation.[3,38] In Sr_2IrO_4, the parameter of the easy-plane anisotropy for the NN interactions, $\Delta_\lambda = 1 - J_{12}^{zz}/J_{12}^{xx}$, has been recently

estimated in the X-ray resonant magnetic scattering experiments as 0.08,[39] which is close to our theoretical value of 0.087. The symmetric anisotropic part of $\overleftrightarrow{\boldsymbol{J}}_{12}$ is $|J_{12}^{(S)xy}| \equiv \Delta J_{12} =$ 0.73 meV, which is about one order of magnitude smaller than in Ba_2IrO_4. This interaction is also bond-dependent.

The antisymmetric part of $\overleftrightarrow{\boldsymbol{J}}_{12}$ can be represented in terms of the of DM vector (in meV): $\boldsymbol{d}_{12} = (-0.1, -0.1, -3.97)$ (see Fig. 1 for the notations of the atomic sites). The phases of d^x and d^y alternate in the four NN bonds around the site 1. Therefore, since all NN atoms, surrounding the site 1, have the same direction of the pseudospin, the total contribution of d^x and d^y to the canting of these pseudospins will vanish. On the other hand, the phases of d^z are the same for all NN bonds. Thus, d^z will be responsible for the ferromagnetic (FM) canting, which can be estimated as $|d_{12}^z/(2J_{12}^{xx})| \sim 2.8°$. This value is smaller than the experimental estimate of 8°.[1] Nevertheless, the negative sign of d^z for the bond 1-2 is consistent with the counterclockwise rotation of the IrO_6 octahedra.[13] This picture can be also verified experimentally.[40]

The g-tensor relates the pseudospins with the value of true magnetic moments, which can be observed in the experiment. Using the value of $g^{xx} = 1.115$ (Table I), the local magnetic moment in the xy plane can be estimated as $\frac{1}{2}g^{xx} = 0.56\ \mu_B$, where the spin and orbital counterparts are $\frac{1}{2}g_S^{xx} = 0.10\ \mu_B$ and $\frac{1}{2}g_L^{xx} = 0.46\ \mu_B$, respectively.

D. Calculations of Néel temperature

Thus, the first-principles calculations have revealed a big difference of the magnetic models in the case of Ba_2IrO_4 and Sr_2IrO_4. On the one hand, the leading isotropic exchange interaction of 123 meV in Ba_2IrO_4 is about three times larger than that of 39 meV in Sr_2IrO_4. In turn, the symmetric anisotropic interaction $J_{12}^{(S)xy}$ in Ba_2IrO_4 is an order of magnitude larger than in Sr_2IrO_4. On the other hand, there is an appreciable DM interaction in Sr_2IrO_4, but not in Ba_2IrO_4. One of the puzzling points is that the experimental Néel temperature remains practically the same in both compounds (about 240 K). The aim of this section is to check whether such striking similarity can be explained using above parameters of interatomic exchange interactions derived in the SE approximation.

Let us first investigate the effect of the DM interaction on the energy spectrum of the pseudospin model. In the $4m/mmm$ coordinate frame, the exchange interaction tensor in

the bond 1-2, which is parallel to the y' axis, is given by

$$\overleftrightarrow{\boldsymbol{J}}_{12} = \begin{pmatrix} J_{12}^{xx} - \Delta J_{12} & -d_{12}^{z} & 0 \\ d_{12}^{z} & J_{12}^{xx} + \Delta J_{12} & 0 \\ 0 & 0 & J_{12}^{zz} \end{pmatrix},$$

where for simplicity we have dropped the small contributions of d_{12}^{x} and d_{12}^{y}. For the bonds parallel to the x' axis, ΔJ_{12} should be replaced by $-\Delta J_{12}$. By considering the transformation,

$$\overleftrightarrow{\boldsymbol{J}}_{12} \rightarrow \overleftrightarrow{\tilde{\boldsymbol{J}}}_{12} = \overleftrightarrow{U}_1 \overleftrightarrow{\boldsymbol{J}}_{12} \overleftrightarrow{U}_2^{T}$$

with

$$\overleftrightarrow{U}_1 = \overleftrightarrow{U}_2^{T} = \begin{pmatrix} \cos\phi & \sin\phi & 0 \\ -\sin\phi & \cos\phi & 0 \\ 0 & 0 & 1 \end{pmatrix}$$

and $\phi = \frac{1}{2}\arctan(d_{12}^{z}/J_{12}^{xx})$ minimizes the energy of DM interactions,[13,41] the tensor $\overleftrightarrow{\boldsymbol{J}}_{12}$ can be transformed to

$$\overleftrightarrow{\tilde{\boldsymbol{J}}}_{12} = \begin{pmatrix} \tilde{J}_{12}^{xx} - \Delta J_{12} & 0 & 0 \\ 0 & \tilde{J}_{12}^{xx} + \Delta J_{12} & 0 \\ 0 & 0 & J_{12}^{zz} \end{pmatrix},$$

where $\tilde{J}_{12}^{xx} = J_{12}^{xx}\sqrt{1 + (d_{12}^{z}/J_{12}^{xx})^2}$. Thus, the DM interactions alone do not confine the pseudospins in any particular directions.[13,41] Moreover, after such transformation to the local coordinate frame, the effect of the DM interactions can be combined with J_{12}^{xx}. Since in the 6-orbital model for Sr_2IrO_4, $d_{12}^{z} = 3.97$ meV while $J_{12}^{xx} = 40.2$ meV, the renormalization of $\tilde{J}_{12}^{xx}$ due to the DM interaction is only about 0.5 %. Therefore, we conclude that the effect of the DM interaction on the energy spectrum is small and can be neglected and, as far as the energy spectrum is concerned, the main ingredients of the pseudospin model are essentially the same in the case of Ba_2IrO_4 and Sr_2IrO_4.

Below, we will concentrate on two mechanisms of the magnetic ordering in iridates: the first one is due to the in-plane anisotropy, which emerges in the 6-orbital model, and the second one is due to the interlayer exchange coupling, which is relevant to the 2-orbital model of Ba_2IrO_4. Thus, we consider the following general compass Heisenberg model

$$\begin{aligned} \hat{\mathcal{H}}_{\mathcal{S}} = \frac{J_z}{2} \sum_{<ij> \text{ in plane}} \mathcal{S}_i^{z}\mathcal{S}_j^{z} + \frac{1}{2}\sum_{<ij>\|x} \left(J_{\|}\mathcal{S}_i^{x}\mathcal{S}_j^{x} + J_{\perp}\mathcal{S}_i^{y}\mathcal{S}_j^{y}\right) \\ + \frac{1}{2}\sum_{<ij>\|y} \left(J_{\|}\mathcal{S}_i^{y}\mathcal{S}_j^{y} + J_{\perp}\mathcal{S}_i^{x}\mathcal{S}_j^{x}\right) + \frac{J'}{2}\sum_{<ij> \text{ inter plane}} \boldsymbol{\mathcal{S}}_i\boldsymbol{\mathcal{S}}_j, \end{aligned} \tag{6}$$

where it is convenient to introduce the shorthand notations: $J_z \equiv J_{12}^{zz}$, $J_\parallel \equiv J_{12}^{xx} + \Delta J_{12}$, $J_\perp \equiv J_{12}^{xx} - \Delta J_{12}$, and J' is the coupling between the atoms, which belong to different planes, separated by the primitive translation c along the z axis. The magnon spectrum of this model for $J' = 0$ was calculated in Ref. 42. It reads

$$E_{\mathbf{q}}^{(1)} = \zeta S \sqrt{(4J_{\rm av} + B_q - A_q)(4J_{\rm av} + B_q + A_q + J_{\rm av} g)},$$
$$E_{\mathbf{q}}^{(2)} = \zeta S \sqrt{(4J_{\rm av} - B_q - A_q + J_{\rm av} g)(4J_{\rm av} - B_q + A_q)}, \tag{7}$$

where $J_{\rm av} = (J_\parallel + J_\perp)/2 = J_{12}^{xx}$,

$$A_{\mathbf{q}} = (J_\perp + J_z)\cos q_x + (J_\parallel + J_z)\cos q_y,$$
$$B_{\mathbf{q}} = (J_\perp - J_z)\cos q_x + (J_\parallel - J_z)\cos q_y, \tag{8}$$

and

$$g = 0.16(J_\parallel - J_\perp)^2/(J_{\rm av}^2 S) = 0.64(\Delta J_{12}/J_{12}^{xx})^2/S \tag{9}$$

is the quantum gap. Moreover, we have introduced the renormalization factor $\zeta = 1 + 0.0785/S$, which is taken equal to its value in the two-dimensional Heisenberg model. Then, for small $\mathbf{q}$ we obtain

$$4J_{\rm av} - B_{\mathbf{q}} - A_{\mathbf{q}} \to J_\perp q_x^2 + J_\parallel q_y^2,$$
$$4J_{\rm av} - B_{\mathbf{q}} + A_{\mathbf{q}} \to 4(J_{\rm av} + J_z),$$
$$4J_{\rm av} + B_{\mathbf{q}} - A_{\mathbf{q}} \to 4(J_{\rm av} - J_z) + J_z q^2 = J_z\left(q^2 + f\right),$$
$$4J_{\rm av} + B_q + A_q \to 8J_{\rm av}, \tag{10}$$

where the parameter f describing the in-plane symmetric anisotropy is defined as

$$f = 4(J_{\rm av} - J_z)/J_z. \tag{11}$$

Therefore, we have:

$$E_{\mathbf{q}}^{(1)} \simeq S\zeta\sqrt{8J_{\rm av} J_z\,(q^2 + f)},$$
$$E_{\mathbf{q}}^{(2)} \simeq S\zeta\sqrt{4(J_{\rm av} + J_z)(J_\perp q_x^2 + J_\parallel q_y^2 + J_{\rm av} g)}. \tag{12}$$

The first mode is related to the out-of-plane pseudospin rotation, while the second corresponds to the in-plane rotation.

To obtain magnetic transition temperatures, we map the Heisenberg model (6) onto the non-linear sigma model, having the same excitation spectrum, Eq. (12), see Appendix.

Treating the magnetic excitations, as slightly different from the case of the XY anisotropy,[43] we obtain in the regime $f \gg \max(\alpha, g)$, $\alpha = 2J'/J$, the following equation for the Neel temperature (see Appendix):

$$T_N = 4\pi\rho_s \left\{ \ln \frac{T_N^2}{c_{\rm op} c_{\rm ip} f_r} + 4 \ln \frac{4\pi\rho_s}{T_N} - \frac{2A^2}{\ln^2 \left(f/\max(\alpha, g) \right)} \right\}^{-1}, \tag{13}$$

where $A \simeq 3.5$, $c_{\rm op} = \sqrt{8 J_{\rm av} J_z} S\zeta$ and $c_{\rm ip} = \sqrt{4 J_{\rm av} (J_{\rm av} + J_z)} S\zeta$ are the out-of-plane and in-plane spin-wave velocities, $\rho_s = 2(1/\rho_{\rm z} + 1/\rho_{\rm av})^{-1}$ is the effective spin stiffness ($\rho_{\rm z,av} = J_{z,{\rm av}} \zeta S \overline{S}_0$), $f_r = f(\overline{S}_0/S)^2$ is the renormalized anisotropy parameter, $\overline{S}_0 = 0.303$ for $S = 1/2$ is the ground-state magnetization. In the absence of compass anisotropy, $f = g = 0$, we obtain instead[44]

$$T_N = 4\pi\rho_s \left\{ \ln \frac{2T_N^2}{c_{\rm op} c_{\rm ip} \alpha_r} + 3 \ln \frac{4\pi\rho_s}{T_N} - 0.06 \right\}^{-1}, \tag{14}$$

where $\alpha_r = \alpha(\overline{S}_0/S)$ is the renormalized interlayer coupling parameter.

The parameters and the resulting magnetic transition temperatures are listed in Table II. Lets us first discuss the results of the 6-orbital models for the Ba_2IrO_4 and Sr_2IrO_4. Judging

TABLE II. Parameters used in Eqs. (13) and (14) for the transition temperature equation and the calculated T_N in different regimes (the values of $J_{\rm av}$, $J_\parallel - J_\perp$, and J_z are in meV, T_N is in Kelvins, and other parameters are dimensionless).

	$J_{\rm av}$	$J_\parallel - J_\perp$	J_z	f	g	α	$c_{\rm op}$	$c_{\rm ip}$	$T_N^{\alpha=0,g=0}$	T_N
Ba_2IrO_4 (2-orb.)	122.8	0	122.8	0	0	$1.4{\cdot}10^{-4}$	200.9	200.9	-	239
Ba_2IrO_4 (6-orb.)	110.6	15	108.1	0.09	$6{\cdot}10^{-3}$	$1.3{\cdot}10^{-4}$	178.9	179.9	371	414
Sr_2IrO_4 (6-orb.)	40.2	1.5	36.7	0.38	$4{\cdot}10^{-4}$	$1.5{\cdot}10^{-5}$	62.8	64.3	181	216

by the ratio between the anisotropy parameters f, g and interlayer isotropic parameter, α, we have the relation $f \gg g \gg \alpha$, which holds for both compounds. Thus, the in-plane anisotropy is expected to be mainly responsible for the magnetic ordering. The differences between in-plane and out-of-plane components of the symmetric anisotropy tensor, $(J_{\rm av} - J_z)$, are close to each other and equal to 2.5 meV (in Ba_2IrO_4) and 3.5 meV (in Sr_2IrO_4). However, due to the difference in the absolute value of J_z, we obtain completely different anisotropy parameters f, g and, therefore, the transition temperatures. For Sr_2IrO_4, the calculated temperature of 216 K is in the good agreement with the experimental value of 240 K. This is consistent with the finding of Jackeli and Khaliullin (Ref. 13), who used

the experimental T_N in order to estimate the values of the exchange interactions and these values are close to ours. However, the situation is different in the case of Ba_2IrO_4, where the theoretical T_N is overestimates by factor two. Interestingly, in the case of the 2-orbital model for Ba_2IrO_4, which, in analogy with the cuprates,[44] contains only in-plane and inter-plane isotropic exchange interactions, we observe a good agreement between theory and experiment. However, this agreement is probably fortuitous.

VI. BEYOND SUPEREXCHANGE

The main purpose of this section is to discuss the effect, which are not included to the regular SE model. Our main concern is the following: since the SE model is based on the second-order perturbation theory for the transfer integrals, it implies that all effects of the SO coupling, which are included to these transfer integrals, are also automatically treated only up to the second order. Since the SO coupling is large in iridates, this may be rather crude approximation, which does not take into account some important anisotropic interactions. For instance, in the mean-field approximation for the SE model, all pseudospins in the single xy plane of Ba_2IrO_4 and Sr_2IrO_4 can rotate rigidly at no energy cost. Besides quantum effects, considered in the previous section (see also Ref. 16), this maybe related to the lack of the in-plane anisotropy, which typically appears only in the fourth order of the SO coupling.

If we wanted to include these effects in the pseudospin model (3), our strategy would be to go beyond the second order perturbation theory for the transfer integrals and consider higher-order terms, which give rise to the new type of interactions, such as biquadratic and ring exchange.[45,46] They will affect both anisotropic and isotropic parts of the exchange interactions. Therefore, in the pseudospin formulation, based on the strong SO coupling, these two types of the effects are connected with each other: if we want to consider the higher order anisotropic interactions, we have to deal with the biquadratic and ring exchange terms, which will affect all other exchange interactions, including the isotropic ones. Such pseudopsin Hamiltonian is no longer presented in the bilinear form (3).

Nevertheless, in the present work we take a different strategy and in order to evaluate the higher-order contributions (and, therefore, check the validity of the SE model) in Ba_2IrO_4 and Sr_2IrO_4, we solve the original electron model (1) in the mean-field HF approximation,

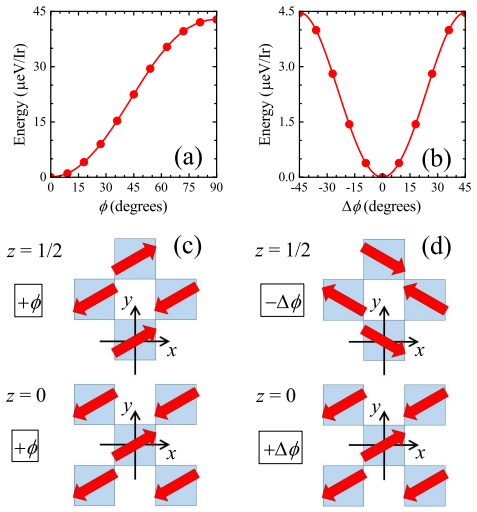

FIG. 7. (Color online) Results of constrained unrestricted Hartree-Fock calculations for Ba_2IrO_4 in the staggered "antiferromagnetic" field $\mu_B H = 0.68$ meV. The direction of the magnetic field in the planes $z = 0$ and $z = 1/2$ is specified by azimuthal angles $(\phi+\Delta\phi)$ and $(\phi-\Delta\phi)$, respectively (in the $I4_1/acd$ coordinate frame). (a) is the total energy dependence on ϕ for $\Delta\phi = 0$. (b) is the total energy dependence on $\Delta\phi$ for $\phi = 0$. (c) and (d) explains the geometry of the staggered magnetic field for (a) and (b), respectively.

where we also apply the staggered external magnetic field, which controls the directions of the spin and orbital moments. We have found that the field of $\mu_B H = 0.68$ meV is generally sufficient for these purposes.

The weak point of the HF approach is that it treats all on-site electron-electron interactions on the mean-field level, whereas in the SE theory such processes are treated rigorously by solving the exact eigenstates problem for the virtual two-hole states. However, in this particular case, we do not expect large error caused by the mean-field approximation (some comparison for transition-metal perovskite oxides can be found in Ref. 25). On the other hand, the HF method does not employ any additional approximations regarding the relative strength of transfer integrals and the on-site Coulomb repulsion and, in this sense, is the more superior approach in comparison with the SE theory.

Let us start with Ba_2IrO_4. The geometry of the constraining field in this case is explained in Fig. 7. First, let us consider the case, where the fields in the two adjacent planes $z = 0$ and $z = 1/2$ are rotated in phase. Then, the total energy exhibits the minimum at $\phi = 0$

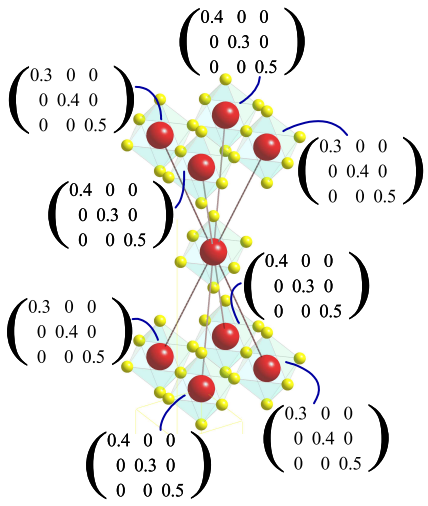

FIG. 8. (Color online) Tensors of superexchange interactions $\overleftrightarrow{J}_{ij}$ (in meV and in the $I4_1/acd$ coordinate frame), associated with different Ir-Ir bonds between adjacent planes in Ba_2IrO_4. The Ir atoms are indicated by the big (red) spheres and the oxygen atoms are indicated by the small (yellow) spheres.

(modulo π, in the $I4_1/acd$ coordinate frame). This effect can be actually included in the SE model and is related to the anisotropy of the exchange interactions between adjacent planes.[16] The behavior of these interactions is explained in Fig. 8. Then, the mean-field energy of the magnetic order, depicted in Fig. 7c, is given by $E(\phi) = -\Delta J_{\rm out} \cos 2\phi$ (per one Ir site), where $\Delta J_{\rm out} = |J^{xx}_{\rm out} - J^{yy}_{\rm out}|$.

Thus, in the SE approximation, the energy should remain invariant with respect to the antiphase rotations of the pseudospin (Fig. 7d). In the other words, if we fix ϕ and consider the configurations, where the directions of the pseudospins in the adjacent planes $z = 0$ and $z = 1/2$ are specified by the azimuthal angles $(\phi+\Delta\phi)$ and $(\phi-\Delta\phi)$, respectively, the mean-field energy of such configurations should not depend on $\Delta\phi$.[16] This property is indeed strictly observed when we use the exchange parameters, derived in the SE model. Because of this degeneracy, the authors of Ref. 16 had to go beyond the mean-field theory and consider the effect of the quantum fluctuations in order to explain the experimentally observed magnetic ground-state structure of Ba_2IrO_4 (corresponding to $\phi = \Delta\phi = 0$ in the $I4_1/acd$ coordinate frame).[15] The most interesting aspect of our analysis is that this degeneracy can be lifted even on the mean-field level if one goes beyond the SE model

and consider more rigorously the higher-order contributions of the transfer integrals in the framework of the unrestricted HF calculations. The dependence of the HF total energy on $\Delta\phi$ is shown in Fig. 8 (for $\phi = 0$). It clearly shows that the higher order-anisotropic interactions, which are included in the HF calculations, lifts the degeneracy and stabilizes the experimentally observed magnetic ground state. The energy barrier, caused by these interactions, is about 4.5 μeV, which is at least comparable with the effect of quantum fluctuations considered in Ref. 16. Thus, the effect is robust and cannot be neglected in the realistic analysis of the magnetic properties of Ba_2IrO_4.

Next, we evaluate the effect of biquadratic exchange on the NN interaction J_{12}^{zz} in the xy-plane of Ba_2IrO_4. If the magnetic properties of some material were indeed described by the bilinear Hamiltonian (3), the values of the exchange parameters would not depend on the method, which is used for their calculations. For instance, in the mean-field HF method, one could evaluate J_{12}^{zz} from the total energy difference between FM and AFM states, by aligning the magnetic moments parallel to the z axis: $J_{12}^{zz} = E_{\uparrow\uparrow} - E_{\uparrow\downarrow}$. Then, if the bilinear parametrization (3) for the magnetic Hamiltonian were indeed appropriate, this value of J_{12}^{zz} should be close to the one obtained in the SE model. Nevertheless, the straightforward HF calculations yield $E_{\uparrow\uparrow} - E_{\uparrow\downarrow} = 83.8$ meV, which is 22% smaller than $J_{12}^{zz} = 108.1$ meV, obtained in the SE model. This deviation is the measure of biquadratic (or ring-type) exchange interactions, existing in the system. Thus, as expected from the discussion in the beginning of this Section, the higher order anisotropic effects in Ba_2IrO_4 coexist with appreciable biquadratic contributions to the isotropic exchange interaction. In this sense, we obtain very consistent description for Ba_2IrO_4. Unfortunately, we could not obtain a stable in-plane FM solution in the HF method and, thus, evaluate the in-plane elements of the exchange tensor from the total energy difference. Generally, one can expect similar contribution of biquadratic interactions to the in-plane and out-of-plane components of the exchange tensor.

The behavior of Sr_2IrO_4 appears to be rather different from Ba_2IrO_4. Since the transfer integrals are smaller in Sr_2IrO_4, while the Coulomb interactions are slightly larger, it is reasonable to expect that the t_{2g} states are more localized in Sr_2IrO_4, which additionally justifies the use of the SE model. This is indeed what we have obtained by comparing results of HF calculations and the SE model. The fact that Ba_2IrO_4 appears to be "more itinerant" than Sr_2IrO_4 can be seen already from the comparison of the band gap, obtained in the

HF method for the AFM ground state, which is substantially smaller in Ba_2IrO_4 (1.3 eV, against 1.8 eV in Sr_2IrO_4). It should be noted, however, that the HF gap is considerably larger than the experimental one, due to the lack of quantum and thermal fluctuations, as was confirmed by the DMFT calculations.[14]

First, we consider the HF solutions for the FM and AFM states, where all magnetic moments are parallel to the z axis. The total energy difference between these states is 31.7 meV, which is much closer to the value $J_{12}^{zz} = 36.7$ meV, obtained in the SE model (the difference is about 14%, which can be again regarded as the measure of biquadratic interactions in the system). In Sr_2IrO_4, it is practically impossible to evaluate the in-plane elements of the exchange tensor from the total energy difference: because of the DM interaction, the in-plane FM state is unstable and converges to the AFM state (with small FM canting of the magnetic moments).

Next, we consider the higher-order anisotropy effects in Sr_2IrO_4. For these purposes we take the weakly FM state and rotate magnetic moments by the external magnetic field of $\mu_B H = 0.68$ meV, which couples to the weak FM moment in the xy plane. The results of such constrained HF calculations are summarized in Fig. 9. We note the following: (i) The total energy depends on the direction of the magnetic moments in the xy plane. However, this dependence is very weak (the characteristic energy barrier is about 0.25 meV, which is an order of magnitude smaller than in Ba_2IrO_4); (ii) The angle ($\Delta\phi$) between magnetic moments of the sites 2 and 1 (see Fig. 1 for the notations) is nearly constant, meaning that it is mainly controlled by the DM interaction d_{12}^z, while the effect of other anisotropic interactions (that are not taken into account in the SE model) are relatively small. Since the energy gain caused by the DM interaction is proportional to $d_{12}^z \sin\Delta\phi$, the obtained values of $-270^\circ < \Delta\phi < -180^\circ$ are well consistent with the sign $d_{12}^z < 0$ of DM interactions for the counterclockwise rotation of the IrO_6 octahedra around the site 1 (see Fig. 1). Yet, one interesting aspect of the HF analysis is that the angle $\Delta\phi$ is different between, separately, spin and orbital magnetic moments. Without external field ($H = 0$), $\Delta\phi$ is about -185.2°. It corresponds to the FM canting of 2.6°, which is close to 2.8°, obtained in the SE model. The values of spin and orbital magnetic moments, obtained for the in-plane (out-of-plane) magnetic alignment are 0.13 and 0.48 μ_B (0.71 and 0.83 μ_B), respectively, which are in good agreement with the values of corresponding matrix elements of the g-tensor, reported in Table I for the SE model.

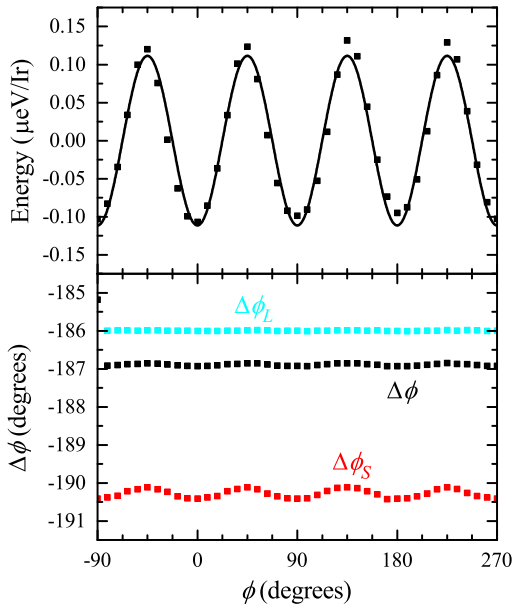

FIG. 9. Results of constrained unrestricted Hartree-Fock calculations for Sr_2IrO_4 in the magnetic field $\mu_B H = 0.68$ meV, which couples to the weak ferromagnetic moment in the xy plane. The direction of the field is specified by the azimuthal angle ϕ. The upper panel displays the behavior of the total energy: the symbols show calculated points, while the solid line is the result of interpolation $E(\phi) = A + B\cos 4\phi$. The lower panel shows the angle between spin ($\Delta\phi_S$), orbital ($\Delta\phi_L$) and total ($\Delta\phi$) magnetic moments of the sites 2 and 1 in Fig. 1.

Thus, we obtain a very consistent description also for Sr_2IrO_4: (i) To a good approximation, the magnetic Hamiltonian has the bilinear form (3), inherent to the SE model; (ii) The higher-order anisotropy effects, beyond the SE model, are negligibly small. This makes the main difference from Ba_2IrO_4, where (i) the deviations from the bilinear form are significant and (ii) the higher-order anisotropic exchange interactions are important.

VII. SUMMARY AND CONCLUSIONS

The main purpose of this work was to critically evaluate the abilities of the SE model for the analysis of magnetic properties of the layered iridates Ba_2IrO_4 and Sr_2IrO_4. Being based on the first-principles electronic structure calculations with the SO coupling, we have first derived the effective low-energy electron model for the t_{2g} bands, which are located near the Fermi level and primarily responsible for the magnetic properties of Ba_2IrO_4 and

Sr_2IrO_4. This electron model was further mapped on the pseudospin model using the theory of SE interactions in the limit of large on-site Coulomb repulsion. We have clarified the microscopic origin of the bond-dependent anisotropic exchange interactions, as well as the antisymmetric DM interactions, caused by the anti-phase rotations of the IrO_6 octahedra in Sr_2IrO_4. The pseudospin Hamiltonian problem has been solved by means of the non-linear sigma model, that has finally allowed to evaluate the Néel temperature for both considered compounds. We have demonstrated that while for Sr_2IrO_4 the theoretical Néel temperature is in good agreement with the experimental data, for Ba_2IrO_4 it is overestimated by factor two. We have argued that this discrepancy is quite consistent with the limitations of the SE model for Ba_2IrO_4, which is the more "itinerant" system than Sr_2IrO_4. Such "itineracy" is directly related to the details of the electronic structure of Ba_2IrO_4: the lack of rotations of the IrO_6 octahedra and the proximity of the Ba $5d$ states to the Fermi level make the t_{2g} bandwidth increase and more efficiently screen the Coulomb interactions in this band. Thus, the $\hat{t}/\mathcal{U}$ expansion for the magnetic energy converges slower and higher-order terms, beyond the SE contributions, start to play an important role. Since the effect of SO interaction in the SE formulation is included to the transfer integrals, the higher-order terms automatically improve the description also for the anisotropic exchange interactions. In fact, by solving the low-energy electron model for Ba_2IrO_4 in the HF approximation, we were able to reproduce the experimental magnetic ground states structure of this compound even on the mean-field level, without invoking to quantum effects.

Acknowledgements. We acknowledge fruitful communication with Alexander Tsirlin. This work is partly supported by the grant of Russian Science Foundation (project No. 14-12-00306).

Appendix: Derivation of the non-linear sigma model for compass Heisenberg model and its renormalization

1. Nonlinear-sigma model

To obtain the action of the continuum model we pass to the coherent state representation for spin operators and represent the corresponding vectors of spin directions following the

standard procedure

$$\boldsymbol{\mathcal{S}}_i = (-1)^i S\mathbf{n}_i\sqrt{1-(\mathbf{L}_i/S)^2} + \mathbf{L}_i, \tag{A.1}$$

where $\mathbf{L}_i \cdot \mathbf{n}_i = 0$, $\mathbf{n}_i^2 = 1$, and the fields $\mathbf{n}_i$ and $\mathbf{L}_i$ represent the staggered and uniform component. Substituting Eq. (A.1) into (6) we obtain the Lagrangian:

$$\begin{aligned}
L[\mathbf{n},\mathbf{L}] = &-\frac{J_z S^2}{2}\sum_{i,\delta} n_i^z n_{i+\delta}^z - \frac{S^2}{2}\sum_{i,\delta_x}\left(J_\parallel n_i^x n_{i+\delta_x}^x + J_\perp n_i^y n_{i+\delta_x}^y\right)\\
&- \frac{S^2}{2}\sum_{i,\delta_y}\left(J_\parallel n_i^y n_{i+\delta_y}^y + J_\perp n_i^x n_{i+\delta_y}^x\right)\\
&+ \frac{1}{2}\sum_{i,\delta}\left(J_z L_i^z L_{i+\delta}^z + (J_z n_z^2 + J_\parallel n_\delta^2 + J_\perp n_{\tilde{\delta}}^2)\frac{\mathbf{L}_i^2 + \mathbf{L}_{i+\delta}^2}{2}\right)\\
&+ \frac{1}{2}\sum_{i,\delta_x}\left(J_\parallel L_i^x L_{i+\delta_x}^x + J_\perp L_i^y L_{i+\delta_x}^y\right)\\
&+ \frac{1}{2}\sum_{i,\delta_y}\left(J_\parallel L_i^y L_{i+\delta_y}^y + J_\perp L_i^x L_{i+\delta_y}^x\right) + i\sum_i \mathbf{L}_i\cdot[\mathbf{n}_i\times\partial_\tau\mathbf{n}_i],
\end{aligned} \tag{A.2}$$

where $n_{\delta_{x,y}} = n_{x,y}, n_{\tilde{\delta}_{x,y}} = n_{y,x}$, and we keep only terms, which do not vanish and give the leading contribution in the continuum limit. Expanding

$$\mathbf{n}_{i+\delta} = \mathbf{n}_i + (\delta\nabla)\mathbf{n}_i + \frac{1}{2}(\delta^a\delta^b\partial_a\partial_b)\mathbf{n}_i + ... \tag{A.3}$$

and similarly for $\mathbf{L}_{i+\delta}$, we obtain:

$$\begin{aligned}
L[\mathbf{n},\mathbf{L}] = &\frac{S^2}{2}\int d^2\mathbf{x}\left[J_z(\nabla n_z)^2 + J_\parallel(\partial_x n_x)^2 + J_\parallel(\partial_y n_y)^2 + J_\perp(\partial_x n_y)^2 + J_\perp(\partial_y n_x)^2 + J_z f n_z^2\right]\\
&+ \frac{1}{2}\int d^2\mathbf{x}\left[2(4J_z + (J_\parallel + J_\perp - 2J_z)(n_x^2 + n_y^2))\mathbf{L}_i^2 + 2(J_\parallel + J_\perp)(L_x^2 + L_y^2)\right]\\
&+ i\mathbf{L}\cdot[\mathbf{n}\times\partial_\tau\mathbf{n}],
\end{aligned} \tag{A.4}$$

where we have defined f according to (11). Performing the integration over $\mathbf{L}$, we find

$$\begin{aligned}
L[\mathbf{n}] = &\frac{S^2}{2}\int d^2\mathbf{x}\left[J_z(\nabla n_z)^2 + J_\parallel(\partial_x n_x)^2 + J_\parallel(\partial_y n_y)^2 + J_\perp(\partial_x n_y)^2 + J_\perp(\partial_y n_x)^2 + J_z f n_z^2\right]\\
&+ \frac{1}{2}\int d^2\mathbf{x}\frac{1}{2(4J_z + (J_\parallel + J_\perp - 2J_z)(n_x^2 + n_y^2))}[\mathbf{n}\times\partial_\tau\mathbf{n}]_z^2\\
&+ \frac{1}{2}\int d^2\mathbf{x}\frac{1}{2(4J_z + (J_\parallel + J_\perp - 2J_z)(1 + n_x^2 + n_y^2))}[\mathbf{n}\times\partial_\tau\mathbf{n}]_x^2\\
&+ \frac{1}{2}\int d^2\mathbf{x}\frac{1}{2(4J_z + (J_\parallel + J_\perp - 2J_z)(1 + n_x^2 + n_y^2))}[\mathbf{n}\times\partial_\tau\mathbf{n}]_y^2.
\end{aligned} \tag{A.5}$$

In the following we assume the preferable direction of magnetic order along the y axis. Representing

$$n_y = \sqrt{1 - n_x^2 - n_z^2} \tag{A.6}$$

and expanding in $n_{x,z}$ we obtain two branches of the magnon spectrum

$$\begin{aligned} E_z^2 &= 4S^2 J_z (J_\parallel + J_\perp) \left(q^2 + f\right), \\ E_x^2 &= 2S^2 (2J_z + J_\parallel + J_\perp)(J_\parallel q_x^2 + J_\perp q_y^2), \end{aligned} \tag{A.7}$$

which coincides with small q expansion of the results of Sec. V D and Ref. 42.

2. Perturbation theory

In the following we concentrate on the classical part of the Lagrangian (A.5), renormalized by the quantum fluctuations,

$$L_{\rm cl}[\mathbf{n}] = \frac{1}{2} \int d^2\mathbf{x} \left\{ \rho_r \left[(\nabla n_z)^2 + f_r n_z^2 \right] + \rho_\parallel \left[(\partial_x n_x)^2 + (\partial_y n_y)^2 \right] + \rho_\perp \left[(\partial_x n_y)^2 + (\partial_y n_x)^2 \right] \right\}. \tag{A.8}$$

In Eq. (A.8) we use the quantum-renormalized spin stiffnesses, $\rho_r = J_z S \overline{S}_0 \zeta$ and $\rho_{\parallel,\perp} = J_{\parallel,\perp} S \overline{S}_0 \zeta$, where $\overline{S}_0 = S - 0.197$ is the ground state magnetization of the square-lattice Heisenberg model, $\zeta = 1 + 0.157/(2S)$ is the exchange parameter renormalization factor, the bare spin stiffnesses anisotropy, and the renormalized easy plane anisotropy $f_r = f\overline{S}_0^2/(S\zeta)^2$. Following the standard procedure[43,47], we assume that the excitations, described by $L_{\rm cl}[\mathbf{n}]$ are cut on the ultriviolet at the momentum $\Lambda_{\rm uv} = T/c$, where $c = \sqrt{8} J S \zeta$ is the renormalized spin-wave velocity; the remaining (non-universal) contribution of the other part of momentum space yields the abovementioned quantum renormalizations.

Assuming again the long-range order along the y-axis, introducing $\pi = (n_x, n_z)$, and using Eq. (A.6), we obtain

$$\begin{aligned} L_{\rm cl}[\mathbf{n}] = \frac{1}{2} \int d^2\mathbf{x} \Big\{ & \rho_r \left[(\nabla \pi_z)^2 + f_r \pi_z^2 \right] + \rho_\parallel (\partial_x \pi_x)^2 + \rho_\perp (\partial_y \pi_x)^2 \\ & + \frac{\rho_\parallel}{1-\pi^2} (\pi \partial_y \pi)^2 + \frac{\rho_\perp}{1-\pi^2} (\pi \partial_x \pi)^2 \Big\} + \frac{T}{2} \int d^2\mathbf{x} \ln(1-\pi^2) - h \int d^2\mathbf{x} \sqrt{1-\pi^2}, \end{aligned} \tag{A.9}$$

where the first term in the second line comes from the integration measure and in the last term we have introduced external magnetic field along y axis, which will be put to zero in

the end. To perform renormalization of Eq. (A.9), we decouple the interactions via the Wick theorem

$$
\begin{aligned}
L_{\rm cl}[\mathbf{n}] = \frac{1}{2}\int d^2\mathbf{x}\left\{\rho_r\left[(\nabla\pi_z)^2 + f_r\pi_z^2\right] + \rho_\parallel(\partial_x\pi_x)^2 + \rho_\perp(\partial_y\pi_x)^2 + \rho_\parallel\langle\pi_a^2\rangle(\partial_y\pi_a)^2\right. \\
\left.+\rho_\perp\langle\pi_a^2\rangle(\partial_x\pi_a)^2 + \rho_\parallel\langle(\partial_y\pi_a)^2\rangle\pi_a^2 + \rho_\perp\langle(\partial_x\pi_a)^2\rangle\pi_a^2\right] \\
+\frac{1}{2}\int d^2\mathbf{x}\left[h\pi^2 + \frac{h}{2}(3\langle\pi_x^2\rangle + \langle\pi_z^2\rangle)\pi_x^2 + \frac{h}{2}(3\langle\pi_z^2\rangle + \langle\pi_x^2\rangle)\pi_z^2 - T\pi^2\right]. \qquad \text{(A.10)}
\end{aligned}
$$

Rescaling the fields

$$
\begin{aligned}
\pi_x &\to Z_x\pi_x, \\
\pi_z &\to Z_z\pi_z,
\end{aligned}
$$

we obtain renormalized parameters:

$$
\begin{aligned}
\rho_R &= Z_z^2\left[\rho_r + \rho_{xy}\langle\pi_z^2\rangle\right], \\
\rho_{\parallel R} &= Z_x^2\left[\rho_\parallel + \rho_\perp\langle\pi_x^2\rangle\right], \\
\rho_{\perp R} &= Z_x^2\left[\rho_\perp + \rho_\parallel\langle\pi_x^2\rangle\right], \\
\rho_R f_R + h_R &= Z_z^2\left[h + \rho_r f_r + T\int\frac{d^2q}{(2\pi)^2}\frac{\rho_\parallel q_y^2 + \rho_\perp q_x^2}{\rho_r(q^2+f_r)+h} - T + \frac{h}{2}(3\langle\pi_z^2\rangle + \langle\pi_x^2\rangle)\right], \\
\rho_{xy,R} g_R + h_R &= Z_x^2\left[h + T\int\frac{d^2q}{(2\pi)^2}\frac{\rho_\parallel q_y^2 + \rho_\perp q_x^2}{\rho_\parallel q_x^2 + \rho_\perp q_y^2 + \rho_{xy}g + h} - T + \frac{h}{2}(3\langle\pi_x^2\rangle + \langle\pi_z^2\rangle)\right],
\end{aligned} \qquad \text{(A.11)}
$$

where $\rho_{xy} = (\rho_\parallel + \rho_\perp)/2$,

$$
\begin{aligned}
\langle{\pi_z}^2\rangle &= T\int\frac{d^2q}{(2\pi)^2}\frac{1}{\rho_r(q^2+f_r)+h}, \\
\langle{\pi_x}^2\rangle &= T\int\frac{d^2q}{(2\pi)^2}\frac{1}{\rho_\parallel q_x^2 + \rho_\perp q_y^2 + \rho_{xy}g + h},
\end{aligned} \qquad \text{(A.12)}
$$

and g_R is the gap, generated for π_x mode, which also contains the non-universal bare value g, determined by the equation (9). From the equations (A.11) we obtain

$$
\begin{aligned}
Z_x &= Z_z = Z, \\
h_R &= Z^2 h\left[1 + \frac{1}{2}(\langle\pi_z^2\rangle + \langle\pi_x^2\rangle)\right], \\
\rho_R f_R &= \rho_r Z^2 f_r\left[1 - \langle\pi_z^2\rangle\right], \\
\rho_{xy,R} g_R &= \rho_{xy,r} Z^2 g\left[1 - \langle\pi_x^2\rangle\right].
\end{aligned} \qquad \text{(A.13)}
$$

Finally, Z is fixed by the condition, that π_y renormalizes the same way, as π_x, which is due to 90° rotation symmetry in the plane. This implies $h_R = Zh$, such that

$$\begin{aligned} Z &= 1 - \frac{1}{2}\left(\langle \pi_z^2 \rangle + \langle \pi_x^2 \rangle\right), \\ \rho_R &\approx \rho_r \left[1 - \langle \pi_x^2 \rangle\right], \\ f_R &\approx f_r \left[1 - 2\langle \pi_z^2 \rangle\right], \\ \rho_{xy,R}/\rho_{xy} &= 1 - \langle \pi_z^2 \rangle, \\ \gamma_R/\gamma = g_R/g &= 1 - 2\langle \pi_x^2 \rangle, \end{aligned} \tag{A.14}$$

where we have introduced $\gamma = (\rho_\parallel - \rho_\perp)/(2\rho_{xy})$ and neglected small anisotropy terms in the second and third lines. Being rewritten through these quantities, the effective Lagrangian reads

$$\begin{aligned} L_R[\mathbf{n}] = \frac{1}{2}\int d^2\mathbf{x} \Big\{ &\rho_R \left[(\nabla \pi_z)^2 + f_r \pi_z^2\right] + \rho_{xy,R}\left[(\nabla \pi_x)^2 + g_R + \gamma_R (\partial_x \pi_x)^2 - \gamma_R (\partial_y \pi_x)^2\right] \\ &+ \frac{\rho_{xy,R}}{1-\pi^2}(\pi \nabla \pi)^2 + \frac{\rho_{xy,R}\gamma_R}{1-\pi^2}\left[(\pi \partial_x \pi)^2 - (\pi \partial_y \pi)^2\right] \Big\}. \end{aligned} \tag{A.15}$$

3. Renormalization group

To perform RG analysis we introduce sharp momentum cutoff at scale Λ and vary Λ from $\Lambda_{\rm uv}$ to the smallest possible scale; in the following we replace accordingly the index R at the renormalized quantities by Λ, denoting explicitly, at which infrared scale they are evaluated. We also assume in the following that $f > g > \alpha$. According to the obtained expressions, we perform renormalization group procedure in two steps. At the first step we integrate degrees of freedom at momenta scales $f_\Lambda^{1/2} < \Lambda < \Lambda_{\rm uv}$. In this range we can neglect small difference between $x-$ and $z-$ modes in equations (A.14) and obtain the standard flow equations of the $O(3)$ non-linear sigma model with small easy-plane anisotropy

$$\begin{aligned} \frac{dt_\Lambda}{d\ln(1/\Lambda)} &= t_\Lambda^2 + t_\Lambda^3, \\ \frac{d\ln Z_\Lambda}{d\ln(1/\Lambda)} &= -t_\Lambda, \\ \frac{d\ln g_\Lambda}{d\ln(1/\Lambda)} &= \frac{d\ln \gamma_\Lambda}{d\ln(1/\Lambda)} = \frac{d\ln f_\Lambda}{d\ln(1/\Lambda)} = -2t_\Lambda, \end{aligned} \tag{A.16}$$

where $t_\Lambda = T/(2\pi\rho_\Lambda)$. In the first Eq. of (A.16) we have added the two-loop term of the $O(3)$ model. The solution of Eqs. (A.16) is well known,

$$
\begin{aligned}
t_\Lambda &= \frac{t_r}{1 - t_r \ln\left(\frac{\Lambda_{\rm uv} t_\Lambda}{\Lambda t_r}\right)}, \\
Z_\Lambda &= \frac{t_r}{t_\Lambda} = 1 - t_r \ln\left(\frac{\Lambda_{\rm uv} t_\Lambda}{\Lambda t_r}\right), \\
\frac{g_\Lambda}{g_r} &= \frac{\gamma_\Lambda}{\gamma} = \frac{f_\Lambda}{f_r} = \left(\frac{t_r}{t_\Lambda}\right)^2 = \left[1 - t_r \ln\left(\frac{\Lambda_{\rm uv} t_\Lambda}{\Lambda t_r}\right)\right]^2,
\end{aligned}
\tag{A.17}
$$

where we have introduced $t_r = T/(2\pi\rho_r)$. The scaling is stoped at $\Lambda = \Lambda_f$, which fulfills $f_{\Lambda_f} = \Lambda_f^2$. The condition $t_{\Lambda_f} = 1$ determines the Kosterlitz-Thouless temperature in the absence of the in-plane anisotropy. At the scales $g_\Lambda^{1/2} < \Lambda < f_\Lambda^{1/2}$ the z-mode is fully gaped, and we obtain behavior of the coupling constants

$$
\begin{aligned}
\frac{dt_{xy,\Lambda}}{d\ln(1/\Lambda)} &= \frac{d\ln f_\Lambda}{d\ln(1/\Lambda)} = 0, \\
\frac{d\ln Z_\Lambda}{d\ln(1/\Lambda)} &= -t_{xy,\Lambda}/2, \\
\frac{d\ln g_\Lambda}{d\ln(1/\Lambda)} &= \frac{d\ln \gamma_\Lambda}{d\ln(1/\Lambda)} = -2t_{xy,\Lambda},
\end{aligned}
\tag{A.18}
$$

which is in the XY universality class. The consideration of this regime is similar to the case of quasi-two-dimensional easy plane model,[43] and yields the result for the Neel temperature in Eq. (13) of the main text.

---

* SOLOVYEV.Igor@nims.go.jp

[1] G. Cao, J. Bolivar, S. McCall, J. E. Crow, and R. P. Guertin, Phys. Rev. B **57**, R11039 (1998).

[2] B. J. Kim, H. Jin, S. J. Moon, J.-Y. Kim, B.-G. Park, C. S. Leem, J. Yu, T. W. Noh, C. Kim, S.-J. Oh, J.-H. Park, V. Durairaj, G. Cao, and E. Rotenberg, Phys. Rev. Lett. **101**, 076402 (2008).

[3] B. J. Kim, H. Ohsumi, T. Komesu, S. Sakai, T. Morita, H. Takagi, and T. Arima, Science **323**, 1329 (2009).

[4] S. Nakatsuji, Y. Machida, Y. Maeno, T. Tayama, T. Sakakibara, J. van Duijn, L. Balicas, J. N. Millican, R. T. Macaluso, and J. Y. Chan, Phys. Rev. Lett. **96**, 087204 (2006).

[5] Y. Okamoto, M. Nohara, H. Aruga-Katori, and H. Takagi, Phys. Rev. Lett. **99**, 137207 (2007).

[6] G. Chen and L. Balents, Phys. Rev. B **78**, 094403 (2008).

[7] X. Wan, A. M. Turner, A. Vishwanath, and S. Y. Savrasov, Phys. Rev. B **83**, 205101 (2011).

[8] X. Liu, T. Berlijn, W.-G. Yin, W. Ku, A. Tsvelik, Y.-J. Kim, H. Gretarsson, Y. Singh, P. Gegenwart, and J. P. Hill, Phys. Rev. B **83**, 220403(R) (2011).

[9] S. K. Choi, R. Coldea, A. N. Kolmogorov, T. Lancaster, I. I. Mazin, S. J. Blundell, P. G. Radaelli, Y. Singh, P. Gegenwart, K. R. Choi, S.-W. Cheong, P. J. Baker, C. Stock, and J. Taylor, Phys. Rev. Lett. **108**, 127204 (2012).

[10] A. Biffin, R. D. Johnson, S. Choi, F. Freund, S. Manni, A. Bombardi, P. Manuel, P. Gegenwart, and R. Coldea, Phys. Rev. B **90**, 205116 (2014).

[11] T. Takayama, A. Kato, R. Dinnebier, J. Nuss, H. Kono, L. S. I. Veiga, G. Fabbris, D. Haskel, and H. Takagi, Phys. Rev. Lett. **114**, 077202 (2015).

[12] A. Kitaev, Ann. Phys. **321**, 2 (2006).

[13] G. Jackeli and G. Khaliullin, Phys. Rev. Lett. **102**, 017205 (2009).

[14] R. Arita, J. Kuneš, A. V. Kozhevnikov, A. G. Eguiluz, and M. Imada, Phys. Rev. Lett. **108**, 086403 (2012).

[15] S. Boseggia, R. Springell, H. C. Walker, H. M. Rønnow, Ch. Rüegg, H. Okabe, M. Isobe, R. S. Perry, S. P. Collins, and D. F. McMorrow, Phys. Rev. Lett. **110**, 117207 (2013).

[16] V. M. Katukuri, V. Yushankhai, L. Siurakshina, J. van den Brink, L. Hozoi, and I. Rousochatzakis, Phys. Rev. X **4**, 021051 (2014).

[17] H. Jin, H. Jeong, T. Ozaki, and J. Yu, Phys. Rev. B **80**, 075112 (2009).

[18] B. H. Kim, G. Khaliullin, and B. I. Min, Phys. Rev. Lett. **109**, 167205 (2012).

[19] J. Igarashi and T. Nagao, Phys. Rev. B **88**, 104406 (2013).

[20] N. B. Perkins, Y. Sizyuk, and P. Wölfle, Phys. Rev. B **89**, 035143 (2014).

[21] H. Okabe, M. Isobe, E. Takayama-Muromachi, A. Koda, S. Takeshita, M. Hiraishi, M. Miyazaki, R. Kadono, Y. Miyake, and J. Akimitsu, Phys. Rev. B **83**, 155118 (2011).

[22] M. K. Crawford, M. A. Subramanian, R. L. Harlow, J. A. Fernandez-Baca, Z. R. Wang, and D. C. Johnston, Phys. Rev. B **49**, 9198 (1994).

[23] N. E. Christensen, International Journal of Quantum Chemistry **25**, 233 (1984).

[24] O. K. Andersen, Phys. Rev. B **12**, 3060 (1975); O. Gunnarsson, O. Jepsen, and O. K. Andersen, *ibid.* **27**, 7144 (1983); O. K. Andersen, Z. Pawlowska, and O. Jepsen, *ibid.* **34**, 5253 (1986).

[25] I. V. Solovyev, J. Phys.: Condens. Matter **20**, 293201 (2008).

[26] N. Marzari and D. Vanderbilt, Phys. Rev. B **56**, 12847 (1997).

[27] I. V. Solovyev, Z. V. Pchelkina, and V. I. Anisimov, Phys. Rev. B **75**, 045110 (2007).

[28] L. Hedin, Phys. Rev. **139**, A796 (1965); F. Aryasetiawan and O. Gunnarsson, Rep. Prog. Phys. **61**, 237 (1998).

[29] F. Aryasetiawan, M. Imada, A. Georges, G. Kotliar, S Biermann, and A. I. Lichtenstein, Phys. Rev. B **70**, 195104 (2004).

[30] I. V. Solovyev, New J. Phys. **11**, 093003 (2009).

[31] N. W. Ashcroft and N. D. Mermin, *Solid State Physics* (Thomson Learning, 1976).

[32] P. W. Anderson, Phys. Rev. **115**, 2 (1959).

[33] All parameters of the model Hamiltonian are available upon request.

[34] A. M. Oleś, G. Khaliullin, P. Horsch, and L. F. Feiner, Phys. Rev. B **72**, 214431 (2005).

[35] J. Kanamori, Prog. Theor. Phys. **30**, 275 (1963).

[36] I. V. Solovyev, Phys. Rev. Lett. **95**, 267205 (2005).

[37] L. Vaugier, H. Jiang, and S. Biermann, Phys. Rev. B **86**, 165105 (2012). T. Ribic, E. Assmann, A. Tóth, and K. Held, *ibid.* **90**, 165105 (2014).

[38] F. Ye, S. Chi, B. C. Chakoumakos, J. A. Fernandez-Baca, T. Qi, and G. Cao, Phys. Rev. B **87**, 140406(R) (2013).

[39] J. G. Vale, S. Boseggia, H. C. Walker, R. Springell, Z. Feng, E. C. Hunter, R. S. Perry, D. Prabhakaran, A. T. Boothroyd, S. P. Collins, H. M. Rønnow, and D. F. McMorrow, Phys. Rev. B **92**, 020406(R) (2015).

[40] V. E. Dmitrienko, E. N. Ovchinnikova, S. P. Collins, G. Nisbet, G. Beutier, Y. O. Kvashnin, V. V. Mazurenko, A. I. Lichtenstein and M. I. Katsnelson, Nature Physics **10**, 202 (2014).

[41] L. Shekhtman, O. Entin-Wohlman and A. Aharony, Phys. Rev. Lett. 69, 836 (1992).

[42] T. Yildirim, A. B. Harris, A. Aharony, and O. Entin-Wohlman, Phys. Rev. B **52**, 10239 (1995).

[43] V. Yu. Irkhin, A. A. Katanin, Phys. Rev. B. **60**, 2990 (1999).

[44] V. Yu. Irkhin, A. A. Katanin, Phys. Rev. B. **55**, 12318 (1997).

[45] E. L. Nagaev, *Magnetics with Complex Magnetic Interactions* (Science, Moscow, 1988).

[46] A. A. Katanin and A. P. Kampf, Phys. Rev. B. **66**, 100403(R) (2002).

[47] S. Chakravarty, B. I. Halperin, and D. R. Nelson Phys. Rev. B **39**, 2344 (1989).